2017

Thermal Analysis of 3D Printed 420 Stainless Steel

Adithya Pothuri
Minnesota State University, Mankato

Thermal Analysis of 3D Printed 420 Stainless Steel

By

Adithya Pothuri

A Thesis Submitted in Partial Fulfillment of the

Requirements for the Degree of

Master of Science in Mechanical Engineering

Minnesota State University, Mankato

Mankato, Minnesota

May 2016

Signature Date (05/06/2016)

Thermal Analysis of 3D Printed 420 Stainless Steel

Adithya Pothuri

This thesis has been examined and approved by the following members of the student's committee.

_____
Advisor (Dr. Patrick Tebbe)

_____
Committee Member (Dr. Shaobiao Cai)

_____
Committee Member (Dr. Kuldeep Agarwal)

Acknowledgements

I would like to thank the Department of Mechanical Engineering at the Minnesota State University, Mankato for providing the perfect environment for continuing my higher education. I would also like to thank my graduate committee, Dr. Patrick Tebbe, Dr. Kuldeep Agarwal, Dr. Shaobiao Cai for their guidance throughout my thesis.

I am grateful for my family members' support throughout my academic career, both financially and emotionally, without which I would not have been able to complete my degree. Additionally, I would also like to thank Mr. Kevin Schull and Mr. Allan Wodtke for providing me assistance with the equipment.

Table of Contents

Page number

List of Figures

Page number

List of Tables

Page number

Thermal Analysis of 3D Printed 420 Stainless Steel

Adithya Pothuri

Master of Science in Mechanical Engineering.

Minnesota State University, Mankato, MN. 2016.

Abstract

Additive manufacturing opens new possibilities in the manufacturing industry. 3D printing is a form of additive manufacturing. 3D printers will have a significant influence over the industrial market, with extremely positive effects in no time. The main aim of this research is to determine the effect of process parameters of Binder Jet manufactured 420 Stainless Steel (420SS) parts on thermal properties such as thermal conductivity. Different parameters, such as layer thickness, sintering time and sintering temperature were varied. A full factorial design of experiment matrix was made by varying these parameters using two levels. Testing showed that different parameters affected the properties in a different manner. Sintering time was very important property as it changed the composition and arrangement of steel and bronze powder during the sintering process. M-flex 3D metal printer by Ex-one was used to print samples of 420SS.

Chapter 1: Introduction

There are many situations in process modeling or design where it would be useful to know the thermal conductivity of steel, and how it would change as a function of temperature. With the lack of a quantitative model, the main resource is to look for a similar composition in published tables of data [1-3]. Assessing the validity of this procedure without a quantitative model is impossible. During the manufacturing process, thermal conductivity will influence the magnitude of the temperature gradients. During heat treatment, conductivity limits the size of the components that can be produced with the microstructure, since transformation depends on the cooling rate and temperature. A suitable model of thermal conductivity should help improve the design of steels [4], since it is a key thermal transport property of material. There are two methods used to measure thermal conductivity - steady state and transient techniques [5-6]. The transient plane source method is used to determine the thermal conductivity value of steel, and was first developed by Gustafsson in 1967 as a non-steady-state method of measuring the thermal conductivity of transparent liquid [7]. Additive Manufacturing (AM) technology is fast gaining research and development focus. They have not only been making a difference in the industrial field, but also biomedical, music and biology as it can quickly and accurately fabricate any 3D model. There are many methods to manufacture metals using additive manufacturing. Powder Bed Fusion (PBF) methods, includes Selective Laser Sintering, Selective Laser Melting, and Electron Beam Melting, which is one of the methods used to produce metal in AM. These methods create parts with polymers and metallic material

[8]. In this research, Binder Jet (BJ) Technology by Ex One Company is used to manufacture specimen. This method works on the principle of chemical adhesion, which creates a green part, which is then sintered and infiltrated to form a fully dense part. The major components that are produced using this method are SS420, SS316. The application parts produced using this technique include mostly rotors, stators, impellers, and prosthetics.

This thesis study how parameters during the binder jet process affect the thermal conductivity of SS420. Small cylindrical disks of stainless steel 420 composites were made by using binder jet technology with layer thicknesses of 100µm and 200µm. These discs were constrained to varying sintering time and sintering temperature. Thermal conductivity value was obtained using TPS 500S, and specimen evaluated under UM microscope for their microstructure.

Chapter 2: Background and Literature Review

2.1 Additive Manufacturing (AM)

Additive manufacturing is a new manufacturing process. It has a family of different technology that builds parts by adding material layer by layer using a digital 3D solid model [9]. In the past, manufacturing a part involved the selection of a larger raw piece of material, which was then machined to achieve the desired result. Traditional manufacturing processes of steels include several processes, such as forming, casting, machining and joining. This is also referred to as subtractive machining, as the material is removed to create the desired piece. Advancement in manufacturing technologies have now made it possible to manufacture parts using an additive method instead of a subtractive method. The ability to additively manufacture products has opened up new possibilities for complex solid parts. The production of small batches or custom parts that were previously too expensive, too complicated, or nearly impossible to manufacture using subtractive have now been made possible relatively quickly and inexpensively.

Additive manufacturing is a manufacturing process where material is added instead of removed. Early systems were an extrusion type. Since then, additive manufacturing technologies have evolved into different types. Some common technologies today are Photopolymerization, Selective Laser Sintering, Fused Deposition Modeling, Laminated Object Manufacturing, and binder jet. Most additive manufacturing processes follow a similar cycle from concept to realization. The sequence follows the eight basic steps listed in **Error! Reference source not found.** [10].

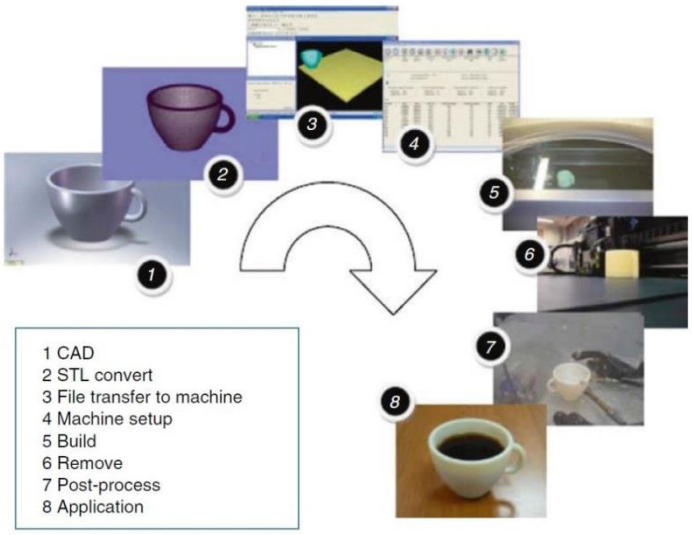

Figure 1. Process Sequence of Additive Manufacturing.

The additive manufacturing process follows the following eight basic steps:

1. Conceptualization and CAD
2. STL Convert
3. Transfer of STL file
4. Machine Setup
5. Build
6. Part removal
7. Post processing of part
8. Application

AM parts must begin from a virtual model designed on software describing the external geometry in detail. The output of the first step should be an STL file format giving information of the exterior surface and the necessary calculations of the slices of the part. In

the next stage, the part is moved to the AM process software, where it is handled according to the AM technology process sequence. The products are carried out layer by layer and according to the CAD model, when some finishing operation is needed after the printing process is done. [11].

Additive Manufacturing eliminates some disadvantages of traditional manufacturing processes:

- Efficient use of resources: Minimizes the processing steps and assembly activities.
- Rapid manufacturing: It has the capability to advance directly from the design process to production phase, which minimizes the tooling process and cycle times.
- Design freedom: It enables designing and producing complex parts with less cost compared to traditional technologies.
- Managing of the complex supply chain is not required as the product is manufactured as a single part.
- The material that is wasted using this method is less compared to traditional manufacturing, as traditional manufacturing involves cutting and machining of material.

Currently, most AM processes are used for low volume prototyping. However, due to increase in technology in this area, it is predicted that AM methods will be used to produce functional parts in near future. Therefore, there is a pressing need for us to know about 3D printed materials more in detail.

In this process, Ex-One M-Flex Metal printer is used; it uses Binder Jetting technology to 3D-print complex parts in industrial-grade materials. Binder Jetting technology uses a liquid

binding agent which is selectively deposited to join powder particles. Liquid binder binds layers of material to form an object by strategically dropping the binder into the powder. The part is printed through the layering of powder and binder. This technology can print a variety of materials like metals, sands and ceramics [12].

Figure 2. Ex One M-Flex 3D metal Printer (12).

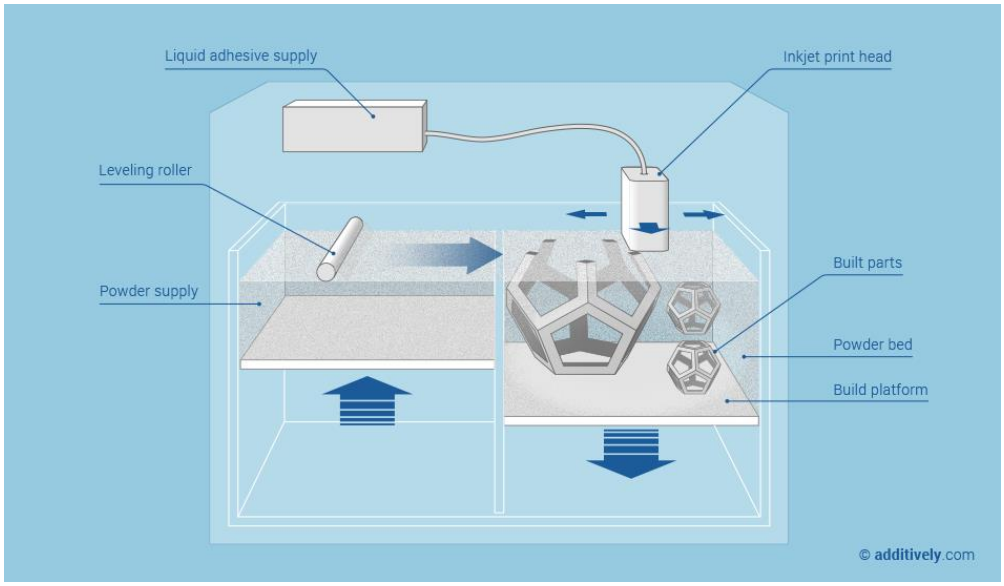

Figure 3. Working overview of M-Flex (12).

2.1.1 General Process

AM involves some steps that move from the virtual CAD description to the resultant physical part. The use of AM is dependant on the type of product. It can be utilized for visualization and also for product development in various stages of manufacturing. Furthermore, early stages of the product development process may only require rough parts, so that design check is done in its early stage. At later stages of the process, parts may require careful cleaning and post-processing, including sanding, surface preparation, and paint before they are finished. Using AM can allow us to manufacture final finished parts that will not require any of the tooling requirements [13].

2.2 Thermal conductivity

Heat transfer from one part of a body to another which is in contact with it is determined as thermal conductivity; it is denoted by K, and it is also defined as the ability of a material to transmit heat. Units for thermal conductivity are watts per square meter of surface area for a temperature gradient of 1k per unit thickness 1m [14]. Fourier's law of heat conduction states that time rate of heat transfer through a material is proportional to thermal conductivity, temperature gradient, and area of the material. Therefore, to successfully measure thermal conductivity, one must be able to measure heat transfer and temperature gradient in materials. Steady state and transient methods are primarily used to measure thermal conductivity.

Thermal conductivity is denoted by K and measured in $W.\mathbf{k^{-1}}.m^{-1}$

Temperature plays a significant role in the thermal conductivity of some materials. The thermal conductivity of some substances varies by a factor of 10 or more for an order of magnitude change in temperature. However, some materials experience little variation in thermal temperature with temperature. Substances affected by temperature have exceedingly high thermal conductivities under low-temperature conditions; these materials are usually referred to as superconductors [15].

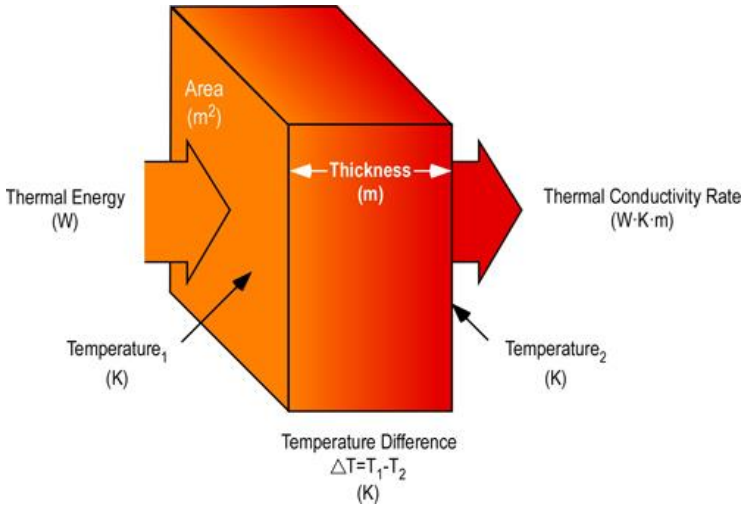

Figure 4. Heat Flow through a block having a thickness m area m².

2.2.1 Thermal Conductivity Equation

Heat conduction H

$$H = \frac{\Delta Q}{\Delta t} = KA\frac{\Delta T}{x} \quad (1)$$

Where $\frac{\Delta Q}{\Delta t}$ is the rate of heat flow, K is the thermal conductivity, A is the total cross-sectional area of conducting surface, ΔT is the temperature difference, and x is the thickness of the conducting surface separating the two temperatures.

$$K = \frac{\Delta Q}{\Delta t}\frac{1}{A}\frac{x}{\Delta T} \quad (2)$$

K is thermal conductivity

$\frac{\Delta Q}{\Delta t}\frac{1}{A}$ Is power per unit area transported

$\frac{\Delta T}{x}$ is the temperature gradient.

ΔQ is thequantity of heat transmitted during time Δt through a thickness x, in a direction normal to a surface of area A, due to temperature difference ΔT, under steady state conditions and when the heat transfer is dependent only on the temperature gradient.

2.2.2 TPS 500S

The thermal conductivity of the printed metal parts is measured using TPS 500S. There are different techniques to measure thermal properties of materials, but Transient Plane Source (TPS) method is one of the most precise. In this approach, the sensor is placed between samples which are equal halves and power is supplied to the sensor. The increase in temperature of the sensor is directly proportional to thermal properties of the material surrounding it. Thermal conductivity value is calculated by TPS 500S taking temperature increase as a function of time [16].

Figure 5. TPS 500S.

During measurement, the sensor is placed between the two halves of the material as shown in figure 6.

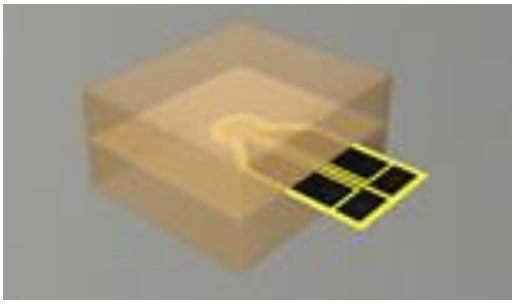

Figure 6. Sensor positioning for TPS 500S (16).

The thermal conductivity equation is based on the assumption that the Hot Disk sensor is located in an infinite medium, which means that the transient measurement must be stopped as soon as the sensor records any influence from the outside boundaries of two sample pieces [16]. Typical sample sizes are between 1 and 10 cm^3, although it can be reduced to 0.01 cm^3 in unique situations. It is important to know that the scale of the flat sample surface should be appreciably larger than the diameter of the hot disk sensor in order not to allow too short a

transient recording. The type of sensor varies with the materials being tested; for metals, the sensor C5501 should be used.

Table 1. Different types of sensors used by Hot Disk.

TPS Sensor Numbers	Measurement Time (seconds)
7577	3
5465	5
5501	10
8563	20

A hot disk sensor is composed of a double spiral structure which is made of nickel wire; this is packed between two thin films of Kapton, as shown in the figure. Kapton serves as electrical insulation, and the sensor assists as both the heat source and the resistance thermometer.

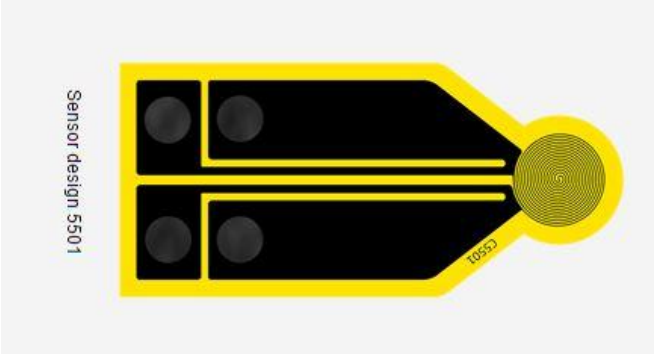

Figure 7. C5501 Sensor.

The sensor is made of a 10µm thick Nickel-metal double spiral. Nickel is used because of its high and well-known temperature coefficient of resistivity. The spiral is supported by a material to protect its particulate shape, increase its strength, and keep it electrically insulated.

This insulation material is Kapton, with a thickness of 12.7µm or 25 µm for temperatures from 30K to 500K, or special Mica insulation with a thickness of around 0.1mm for temperatures between 500K and 1000. The accuracy of thermal conductivities in within +/- 5% and reproducibility is within +/- 2% [17]. The table below gives the specification of TPS 500S

Table 2. TPS Limitations and Parameters.

Thermal Conductivity	0.03 to 100 W/m/K using standard isotropic method 5 to 200 W/m/K using slab or one-dimensional methods
Thermal Diffusivity	0.02 to 40 mm^2/s using standard isotropic method 2 to 100 mm^2/s using slab or one-dimensional methods
Specific Heat Capacity	0.10 to 4.5 MJ/m^3K
Measurement Time	2.5 to 2560 sec
Reproducibility	2 % (thermal conductivity) 10 % (thermal diffusivity, sensor radius 6.4 mm) 12 % (volumetric specific heat, sensor radius 6.4 mm)
Accuracy	Better than 5% (thermal conductivity)
Sensor Types Available	Kapton sensors: 7577, 5465, 5501

2.2.3 Working of TPS 500S with solids:

TPS 500 S is capable of finding the thermal transport properties of isotropic materials. Before starting the experiment, the following inputs are required: measurement time [Sec], heating

power [Watts], test sample temperature [^{o} C], sensor type, sensor material type, sensor design, probing depth, start point, and end point.

Table 3 gives the ideal values of the input parameters for solids:

Table 3. TPS Experimental Parameters.

Input Parameters	Range
Measurement Time	10 sec
Heating Power	1-1.5Watts
Test Sample Temperature	Ambient temperature
Sensor Type	Disk
Sensor Material Type	Kapton
Sensor Design	C5501, radius 6.2 mm
Probing depth	10 mm(varies)
Start Point	12
End Point	200

To begin the experiment, turn on TPS 500S. The unit should be started 60 minutes before the experiment. Input all the input parameters and click "start" to begin the experiment. TPS 500S heats the sample with the selected power, and at the same time, records 200 data points of the temperature increase of the sensor. This recording of temperature increase is known as Transient recording. The sample used in this experiment are finite, to specify the boundary

limit we use probe depth. Two graphs Drift graph and Transient graph are displayed when transient recording is completed.

2.2.4 Drift Graph: Drift graph displays the measured temperature sensor increase before heating. In the chart, the x-axis is time [sec] and y- axis is temperature increase [k]. The measured sensor temperature increase before heating should show small variations. If the sample is still cooling down from the previous experiment, the graph will reflect this. The experiment should be performed when the sample is isothermal, and there is no drift temperature present, as shown in Figure 8.

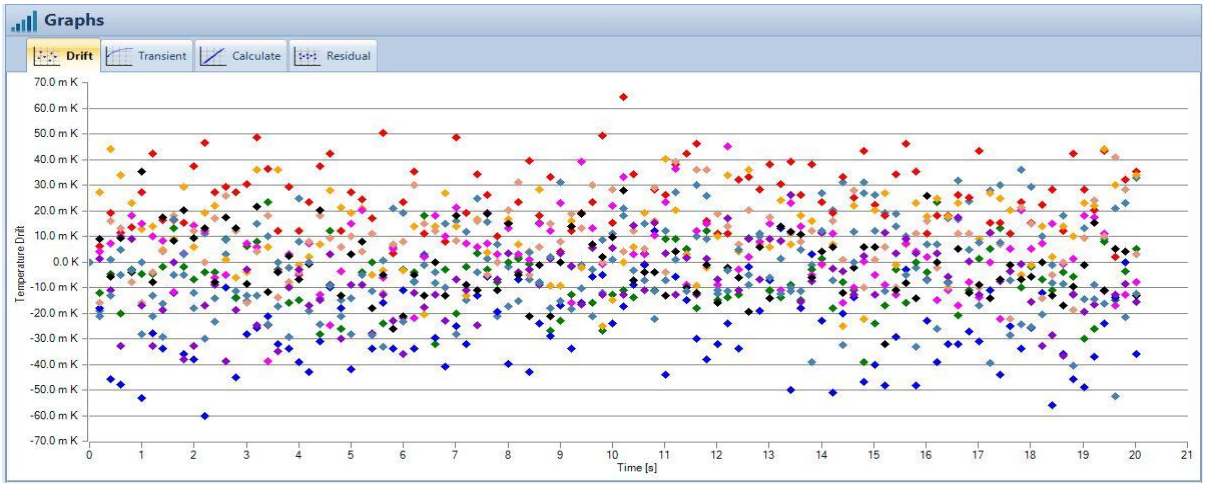

Figure 8. Drift Graph.

2.2.5 Transient graph: It is a temperature increase vs. time [sec] graph. The graph displays the measured sensor temperature while heating the sample. It shows all the 200 points which are recorded to calculate the thermal properties of the sample.

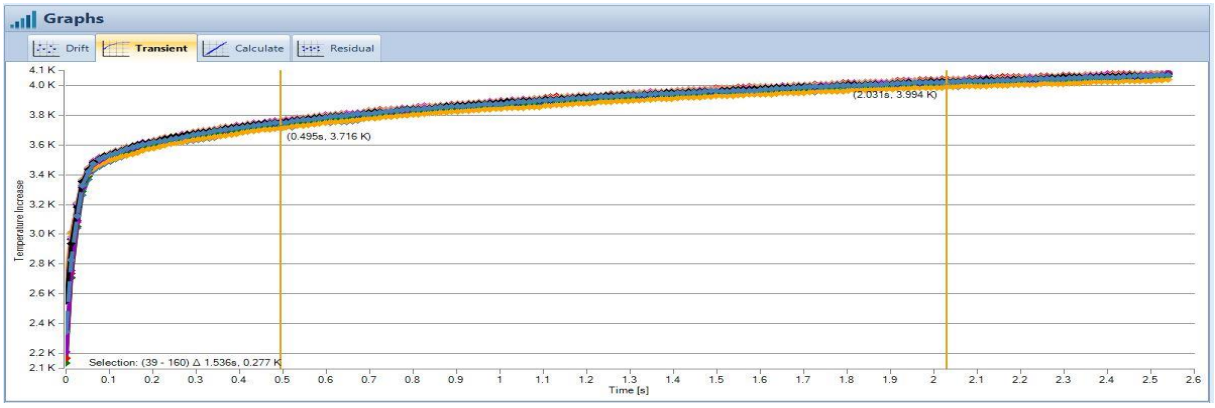

Figure 9. Transient Graph.

After the transient recording is completed and a drift graph and a transient graph are displayed, click on "Calculate" button to find the thermal properties of the 420SS. Enter start point as "10" and end point "200" and click on "standard analysis". Once the selection process is done, results are displayed in a tabular form on the screen, which is shown in Figure 10.

Numeric Results

Thermal Condu...	Thermal Diffusi...	Specific Heat	Probing Depth	Temperature I...	Temperature D...	Total to Charac...	Total Temperat...	Time Correction	Mean Deviation	Sensor Resista...
23.89 W/mK	8.306 mm²/s	2.877 MJ/m³K	8.21 mm	0.280 K	-	0.411	4.04 K	2.732e-005 s	2.664e-003 K	12.709122 Ω
23.90 W/mK	4.937 mm²/s	4.841 MJ/m³K	6.33 mm	0.283 K	-	0.244	4.06 K	0.100 s	2.219e-003 K	12.713407 Ω
23.19 W/mK	4.227 mm²/s	5.486 MJ/m³K	5.86 mm	0.289 K	-	0.209	4.09 K	0.100 s	2.175e-003 K	12.715799 Ω
24.33 W/mK	5.125 mm²/s	4.747 MJ/m³K	6.45 mm	0.283 K	-	0.254	4.04 K	0.1000 s	1.885e-003 K	12.721799 Ω
25.79 W/mK	7.564 mm²/s	3.409 MJ/m³K	7.84 mm	0.265 K	-	0.374	2.81 K	0.0382 s	2.434e-003 K	12.725693 Ω
24.09 W/mK	5.404 mm²/s	4.457 MJ/m³K	6.63 mm	0.282 K	-	0.267	4.07 K	0.0636 s	2.343e-003 K	12.655409 Ω
24.35 W/mK	4.859 mm²/s	5.012 MJ/m³K	6.28 mm	0.279 K	-	0.240	4.08 K	0.100 s	1.925e-003 K	12.658071 Ω
23.40 W/mK	6.287 mm²/s	3.722 MJ/m³K	7.15 mm	0.282 K	-	0.311	4.08 K	1.643e-005 s	2.175e-003 K	12.661053 Ω
23.77 W/mK	6.566 mm²/s	3.620 MJ/m³K	7.30 mm	0.276 K	-	0.325	4.08 K	1.130e-013 s	2.511e-003 K	12.665063 Ω
25.23 W/mK	6.954 mm²/s	3.628 MJ/m³K	7.52 mm	0.277 K	-	0.344	4.08 K	0.0636 s	2.271e-003 K	12.667802 Ω
24.18 W/mK	4.629 mm²/s	5.225 MJ/m³K	6.13 mm	0.276 K	-	0.229	4.07 K	0.100 s	2.533e-003 K	12.670779 Ω
24.193	5.8961	4.2749	6.8828	0.27932	NaN	0.29176	3.9544	0.060498	0.0022849	12.688
0.71753	1.2625	0.8171	0.72979	0.0056783	0	0.062472	0.36332	0.04188	0.00023355	0.027536

Figure 10. Calculated results.

Numeric Results

Thermal Condu...	Thermal Diffusi...	Specific Heat	Probing Depth	Temperature I...	Temperature D...	Total to Charac...	Total Temperat...	Time Correction	Mean Deviation	Sensor Resista...
23.89 W/mK	8.306 mm^2/s	2.877 MJ/m^3K	8.21 mm	0.280 K	-	0.411	4.04 K	2.732e-005 s	2.664e-003 K	12.709122 Ω
23.90 W/mK	4.937 mm^2/s	4.841 MJ/m^3K	6.33 mm	0.283 K	-	0.244	4.06 K	0.100 s	2.219e-003 K	12.713407 Ω
23.19 W/mK	4.227 mm^2/s	5.486 MJ/m^3K	5.86 mm	0.289 K	-	0.209	4.09 K	0.100 s	2.175e-003 K	12.715799 Ω
24.33 W/mK	5.125 mm^2/s	4.747 MJ/m^3K	6.45 mm	0.283 K	-	0.254	4.04 K	0.1000 s	1.885e-003 K	12.721799 Ω
25.79 W/mK	7.564 mm^2/s	3.409 MJ/m^3K	7.84 mm	0.265 K	-	0.374	2.81 K	0.0382 s	2.434e-003 K	12.725693 Ω
24.09 W/mK	5.404 mm^2/s	4.457 MJ/m^3K	6.63 mm	0.282 K	-	0.267	4.07 K	0.0636 s	2.343e-003 K	12.655409 Ω
24.35 W/mK	4.859 mm^2/s	5.012 MJ/m^3K	6.28 mm	0.279 K	-	0.240	4.08 K	0.100 s	1.925e-003 K	12.658071 Ω
23.40 W/mK	6.287 mm^2/s	3.722 MJ/m^3K	7.15 mm	0.282 K	-	0.311	4.08 K	1.643e-005 s	2.175e-003 K	12.661053 Ω
23.77 W/mK	6.566 mm^2/s	3.620 MJ/m^3K	7.30 mm	0.276 K	-	0.325	4.08 K	1.130e-013 s	2.511e-003 K	12.665063 Ω
25.23 W/mK	6.954 mm^2/s	3.628 MJ/m^3K	7.52 mm	0.277 K	-	0.344	4.08 K	0.0636 s	2.271e-003 K	12.667802 Ω
24.18 W/mK	4.629 mm^2/s	5.225 MJ/m^3K	6.13 mm	0.276 K	-	0.229	4.07 K	0.100 s	2.533e-003 K	12.670779 Ω
24.193	5.8961	4.2749	6.8828	0.27932	NaN	0.29176	3.9544	0.060498	0.0022849	12.688
0.71753	1.2625	0.8171	0.72979	0.0056783	0	0.062472	0.36332	0.04188	0.00023355	0.027536

2.2.6 Residual Plot:

The strength of the Hot Disk TPS technique is that it can identify and remove the effect of contact resistance on measurements. The presence of contact resistance on a measurement can be identified by looking at the residual plot in the Hot Disk software.

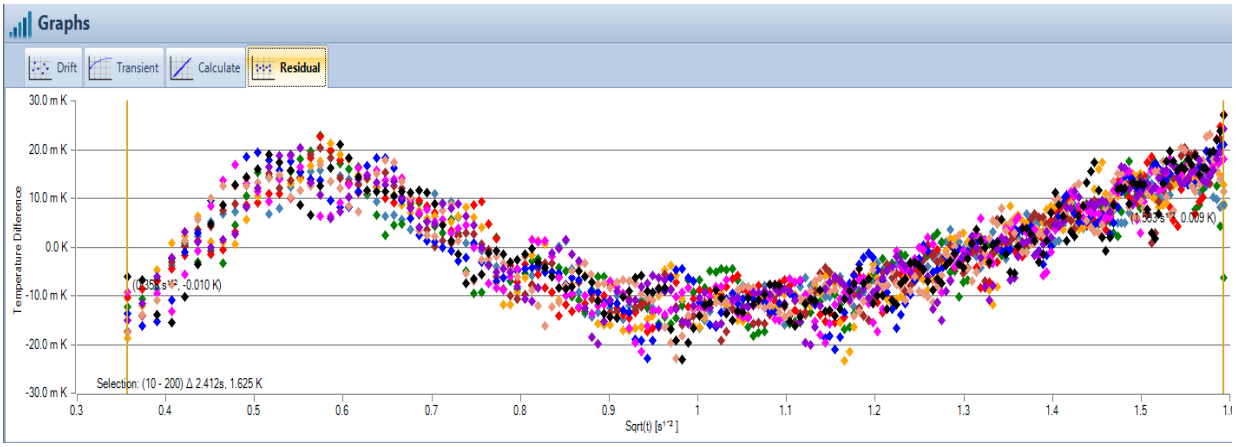

Figure 11. Residual Graph.

2.2.7 Probing Depth: The critical assumption on which the solution of the thermal conductivity equation is based is that the sensor is located in an infinite material. This means that the total time of the transient recording is limited by the presence of outside boundaries or limited size of the sample. In other words, "thermal penetration depth" generated in an experiment must not reach the outside boundaries of the sample pieces during transient recording. An estimation of how far this thermal wave has proceeded in the sample during a recording is the so-called probing depth.

$$\Delta_p = 2.\sqrt{\kappa.t} \quad (3)$$

Where:

K= thermal diffusivity

t= measuring time

The relationship between the probing depth and the total measuring time of the experiment indicates that it is easier to make measurements on larger samples. To determine both thermal conductivity and thermal diffusivity with accuracy, the thickness of a flat sample should not be less than the radius of the hot disk sensor.

Taking input parameters into consideration, a 3D-printed sample is prepared with a diameter of 28.4mm and thickness 9mm.

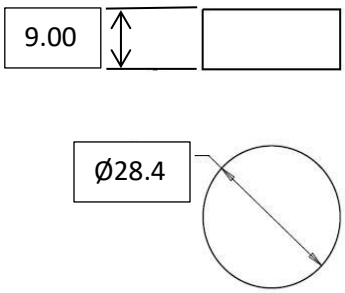

Figure 12. Drawing of Specimen.

Chapter 3: Experimentation

3.1 Design of Experiment

DOE (Design of Experiments) provides an effective means to achieve breakthrough improvements in production quality and process efficiency. From the viewpoint of the industrial field, this can reduce the number of experiments when considering the factors affecting experimental results. DOE can show how to carry out the least number of tests while retaining the most important data. The most important method of the DOE is determining the independent variable. For this purpose, Taguchi [18] introduced an improved DOE. This approach adopts the fundamental idea of DOE, but simplifies and controls factorial and fractional factorial designs so that the experiments can produce more uniform results [19].

In this experiment, the number of factors affecting the final outputs is three and the numbers of levels of each factor are two. Factors considered are layer thickness, sintering time, and sintering temperature, as they have an impact on manufactured specimen sintering process.

Sintering is the process by which lose metal powders are transformed into solids at temperatures below their melting point. In this process, diffusion of material takes place, which results in its mechanical strength.

Layer thickness gives us the thickness of the printed layer by the machine during the process of manufacturing; change in layer thickness will alter the arrangement of the metal powder partials during the process of printing.

Sintering temperature and sintering time are the temperature at which the manufactured specimen is heated and sintering time represents the amount of time sintering is done.

3 factor two-level full factorial DOE is used in my experimentation.

Table 4. Factors and Levels of Experiment Sample.

Factors	Low-Level	High-Level
Layer Thickness	100µm	200 µm
Sintering Temperature	1120°C	1180°C
Sintering Time	90'	180 '

3.1.1 Two level full factorial designs:

Two-level full factorial design is also known as 2^3 factorial design. This method has a total of eight runs; it is represented graphically as shown in figure 13; the arrows determine the direction of increase of the factors.

X1, X2, X3 are layer thickness, sintering time, and sintering temperature.

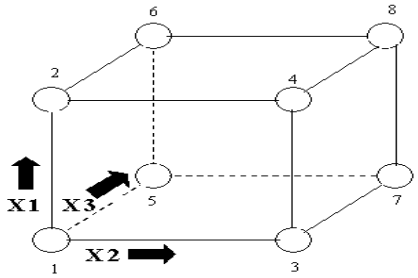

Figure 13. Two-level full factorial design.

With layer thickness, sintering time and sintering temperature as factors, two-level full factorial design combinations can be shown as in table 5.

Table 5. A 2^3 two-level, full factorial design table showing runs in standard order.

Run	Layer thickness	Sintering Temperature	Sintering Time
1	-1	-1	-1
2	1	-1	-1
3	-1	1	-1
4	1	1	-1
5	-1	-1	1
6	1	-1	1
7	-1	1	1
8	1	1	1

Here, -1 represents a low-level of the factor, and 1 accounts for a high-level of the factor.

Table 6. Two-Level Full Factorial for Experiment.

Run	Layer thickness(μm)	Sintering Temperature(°C)	Sintering Time(')
1	100	1120	90
2	200	1120	90
3	100	1180	90
4	200	1180	90
5	100	1120	180
6	200	1120	180
7	100	1180	180
8	200	1180	180

Thermal conductivity parameter was examined in this research, and thermal analysis was done on the printed parts for layer thickness, sintering temperature and sintering time. Each test was performed for 110 minutes for each sample, with 20-minutes intervals between each experiment. The material composition of the sample is 90/10 bronze and 420 Stainless Steel (420SS).

3.2 Sample Preparation

The discs are printed using M-Flex 3D printer by Ex One. The discs were 28.4mm in diameter, with a 10mm thickness. The material diameter is 28.4mm because of the testing parameters of TPS 500S, and this allows two prints at once.

Initially, the binder and cleaner bottles are filled, and the waste (collection) bottle emptied. The system is turned on, after which the white ‘to enable’ button on the front panel is pressed.

To get good samples, we must make sure that the setup is working without a problem. First, the printhead is tested, and then the powder loaded into the machine for printing. The typical steps for print are listed below:

Print head startup and testing

1. Select Print head setup from Main Screen
2. Perform 2 Automatic Cleaning cycles, by pressing Start.
3. Perform Missing Jet Identification and Correction
4. Perform Drop Volume and Saturation

Load powder into the machine for printing

1. Return to the Main Screen.
2. Click on the Powder Setup button.
3. Raise the Build Box to 40 mm, and place build plate in build box. Adjust level as required.
4. Lower the Feed Box to the bottom, at 25 mm.
5. Fill the Feed Box and put some powder on the Build side as well.
6. Spread powder until it is level on both sides.
7. Exit, returning to the Main Screen.

Load part file

1. From the Main Screen, select part selection tap.

2. Open part file that is to be printed.

3. Rotate and scale part.

4. View part layers (ensures STL quality).

5. Repeat for other parts or add copy of original part.

6. Place parts in build envelope.

7. When completed, exit out to the Main Screen.

Printing

1. Close hood.

2. From the Main Screen, start print job.

3. Verify default spread and dry settings.

4. Allow job to print about ten layers; then, if part files have some mass, we can gradually increase spread speed and decrease drying times.

Post print operation

1. Remove build (using jig).

2. Cure parts for 3 hours at 175ºC.

3. Clean up printer (short-term layup).

4. Clean print head by running one automatic cleaning cycle.

5. Clean out tubing by shutting down software and allowing the cleaning cycle to run.

6. Re-fill binder and cleaner bottles and empty the waste bottle.

Initially, the powder is added into the build area as shown in figure 13. Once the print head is tested, the pattern is determined, and the machine is set for printing. In this research, the samples printed using M-Flex metal printer had different layer thickness. Four sample pairs of 100µm and 200µm are printed as shown in Figure 22.

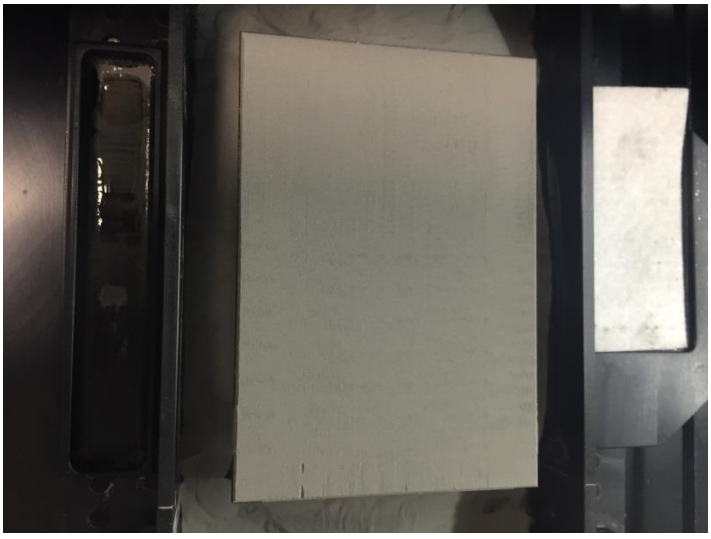

Figure 14. Build area of the M- Flex metal printer.

The binder is spread over the powder metal, and a layer of powder is spread on it. This process is repeated until the sample is completed. This process gives us a green product which can be easily broken, as shown in figure 15.

Figure 15. Binder deposition on the powder metal.

Using a brush, remove all powder from the top portion of the powder box. Use the part removal tool to remove the contents of the build box. Once the part completes its printing process, it is cleaned, and will be ready for curing as shown in figure 15.

Figure 16. Printed Green Part by M-Flex Metal Printer.

Once the green part is cleaned, it is ready for curing; powder used to print must be sieved before using again. In the curing process, time is limited to 3 hours and temperature to 175ºC. This helps the binder evaporate and makes the sample powder bind with greater bond strength, as shown in figure 16.

Figure 17. Sample obtained after curing.

This part is sintered and infiltrated with bronze, which is 90% Copper and 10% Tin. This is done using two sintering temperatures - 1120ºC and 1180ºC - with varying sintering time for each sample, which is 90 minutes and 180 minutes.

Samples are placed in a mixture of Silicate Nitrate, which helps the heat flow be evenly distributed throughout the area. The samples are sintered by placing them in a furnace for 1.5 hours and 3 hours; once they are done, the batch is cooled down before removing them from the chamber. The sample is shown in figure 19.

Figure 18. Furnace.

Figure 19. Silica Nitrate.

Figure 20. Sample obtained after infiltration of bronze.

Samples are sintered with bronze, which has 90% Cu and 10% Sn. Once infiltration is done, disks are removed by machining.

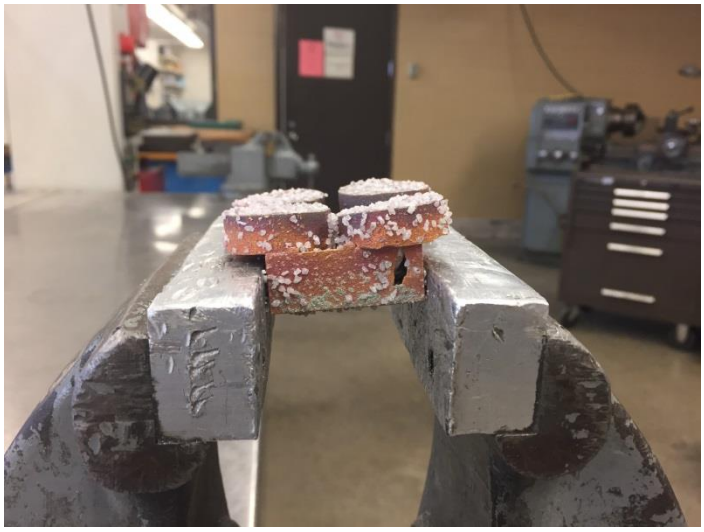

Figure 21. Removing Samples after Infiltration of Bronze.

Then, each sample is machined on a lathe to obtain a smooth surface on one side as required for thermal conductivity testing using TPS 500S.

Figure 22. 420 Stainless steel after machining.

Each sample is machined and surface grinded using wet sanding process with 120, 180, 400, 600 grit to obtain a smooth surface on one side which would be used for testing thermal conductivity using TPS 500S.

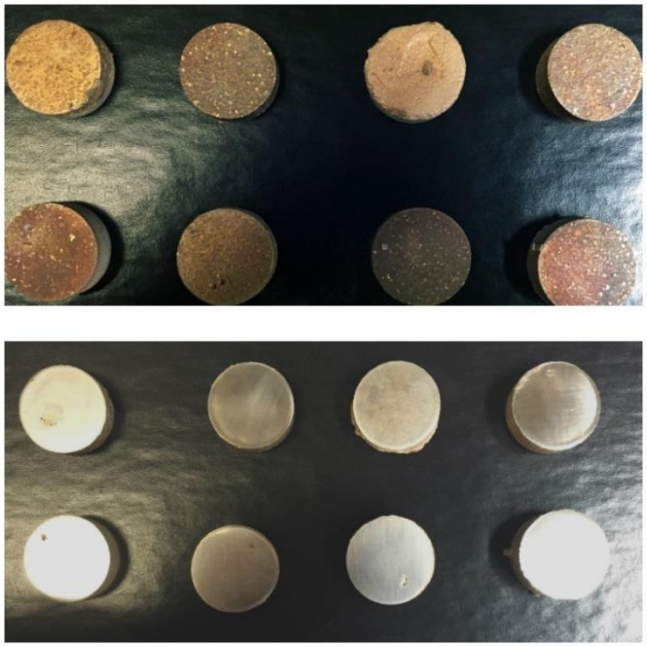

Figure 23. Disks before and after finishing machining.

3.3 Number of Experiments

The number of experiments (11) is determined using statistical analysis.

Using Equation

$$n = \left(\frac{Z_{\frac{\alpha}{2}} * \sigma}{E}\right)^2 \quad (4)$$

n = number of experiments

Z (∝/2) = Confidence interval value

E = Error in Uncertainty, and

σ = Standard deviation

In this case, confidence interval is taken as 95%, E is taken as 0.3, and σ is taken as 0.5.

Each sample is tested 11 times, and the average value of thermal conductivity is taken into consideration.

3.4 Thermal Conductivity Testing

The thermal conductivity of each set of samples is determined using TPS 500S. Each set is placed on one side of the sensor, and the input parameters are given, which are power 1W, time 2.5 seconds, probe depth 9mm, and 11 experiments are run with 20 minutes' gap between each experiment. Thus, thermal conductivity data is obtained for all eight samples.

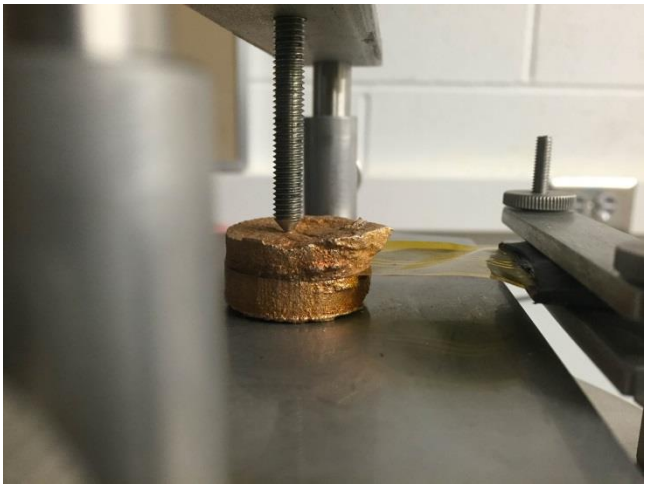

Figure 24. Sample Setup Side View.

Figure 25. Sample Setup top view.

All the data values can be exported to an excel sheet using hot disk software; the time gap between each experiment will have a positive effect on the thermal conductivity value accuracy.

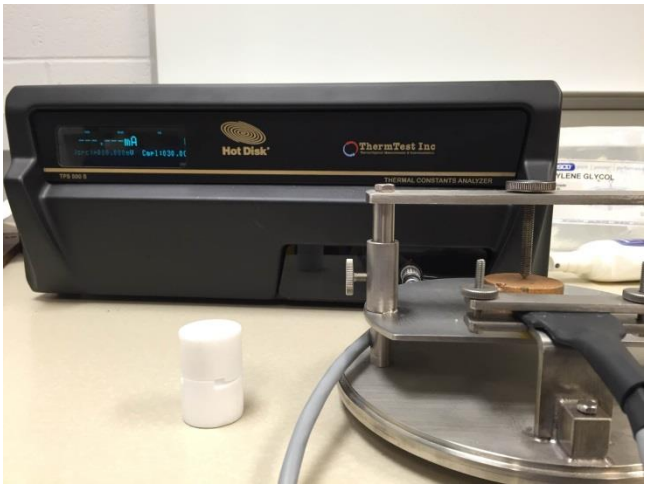

Figure 26. Hot Disk Set-Up.

Table 7. Data obtained from TPS 500S for 200 µm 1.5 hours 1180ºC sintered sample.

Description	Temperature (ºC)	Thermal Conductivity (W/mK)	Thermal Diffusivity (mm^2/s)	Specific Heat (MJ/m^3K)
200µ/1.5hr/1180ºC	22	22.13	26.37	0.84
	22	22.11	25.20	0.88
	22	22.20	24.84	0.89
	22	22.21	24.22	0.92
	22	21.78	26.98	0.80
	22	22.28	22.51	0.99
	22	21.85	26.28	0.83
	22	21.98	26.49	0.83
	22	21.85	26.08	0.81
	22	21.80	26.80	0.89
	22	22.07	24.90	0.87

Average thermal conductivity 22.02 W/mK

Standard Deviation 0.17 W/mK

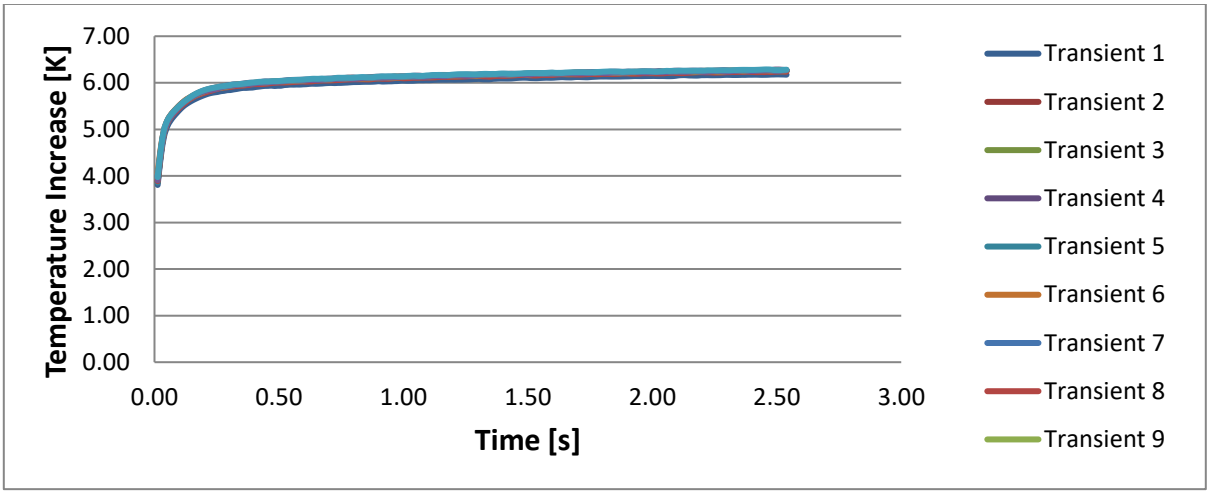

Figure 27. Transient Chart.

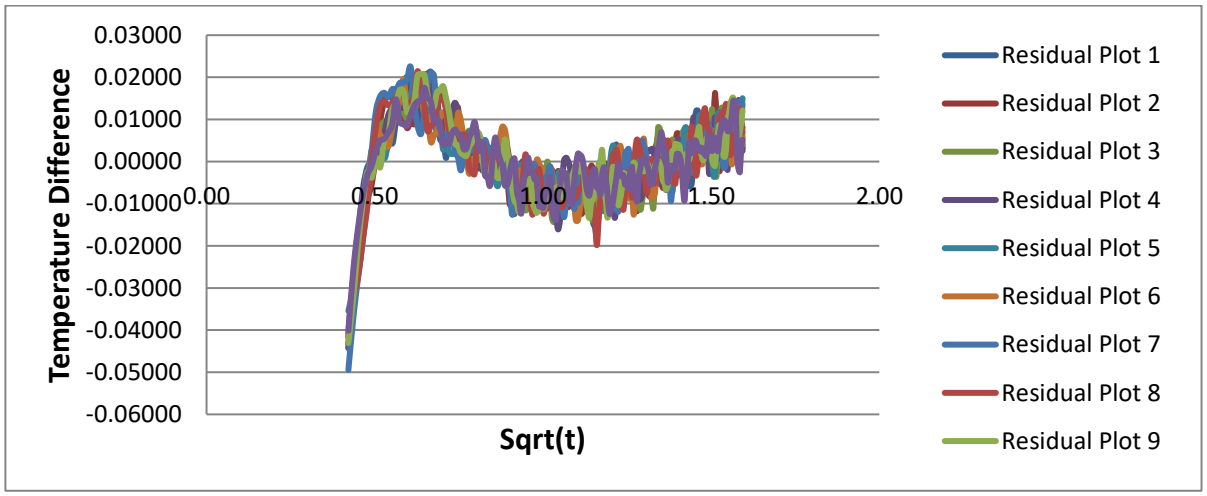

Figure 28. Residual Plot.

3.4.1 Contact Resistance and the Hot Disk TPS Technique

The strength of the Hot Disk TPS technique is that it can identify and remove the effect of contact resistance on measurements. The presence of contact resistance on a measurement can be identified by looking at the residual plot in the Hot Disk software. If a measurement is free and clear of contact resistance, the residual will be randomly scattered. The pictures below show the removal of more and more data points from the front of the analysis, and how the residual changes shape and becomes more randomly scattered as more data points are removed.

Residual 1: Data Points 10 – 200

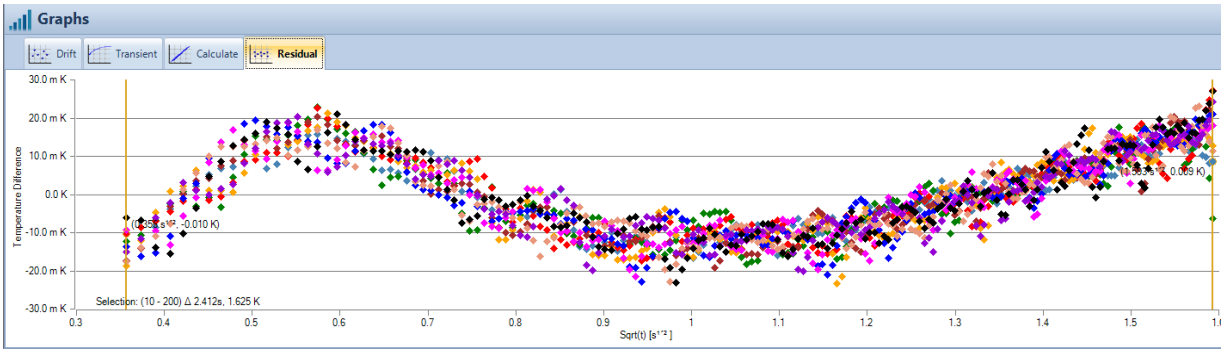

Figure 29. Data points from 10-200.

Residual 2: Data Points 20 – 200

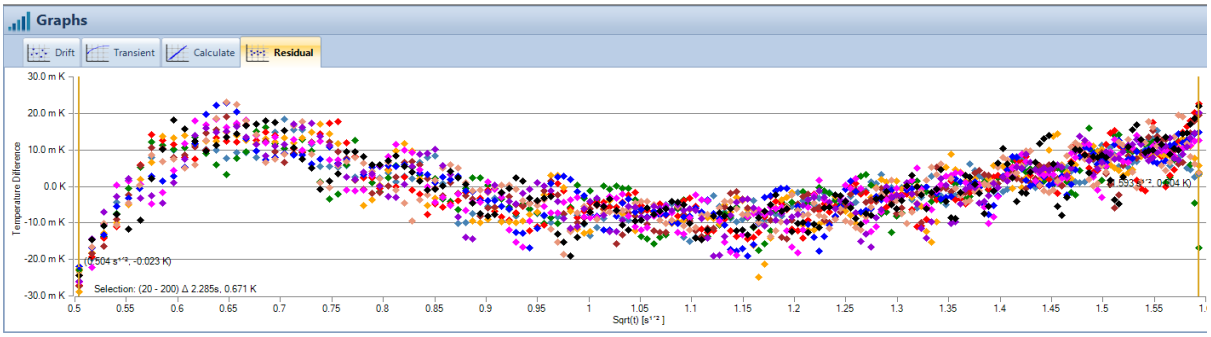

Figure 30. Data points from 20-200.

Residual 3: Data Points 30 – 195

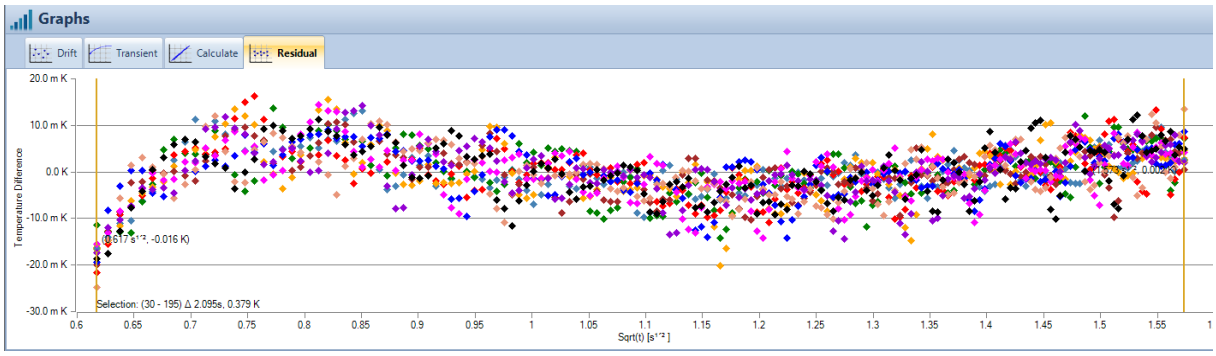

Figure 31. Data points from 30-195.

Residual 4: Data Points 40 – 195

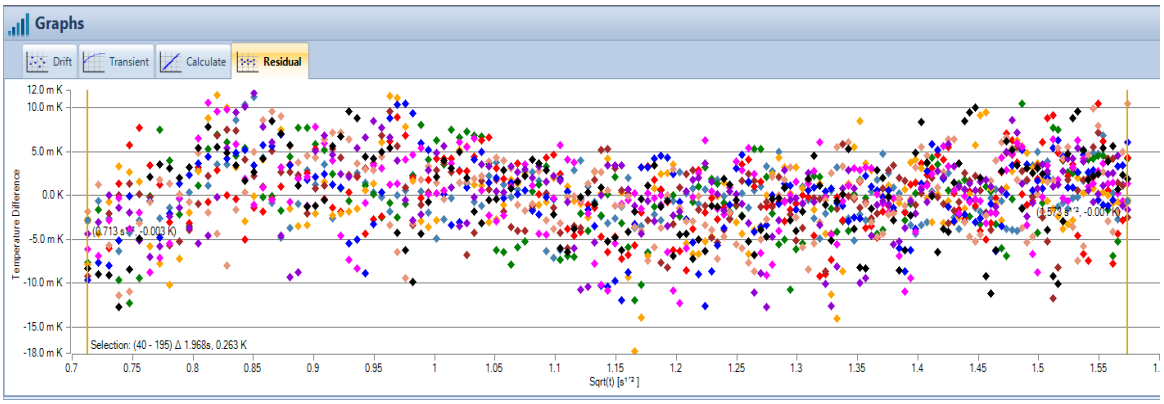

Figure 32. Data points from 40-195.

Residual 5: Data Points 50 -195

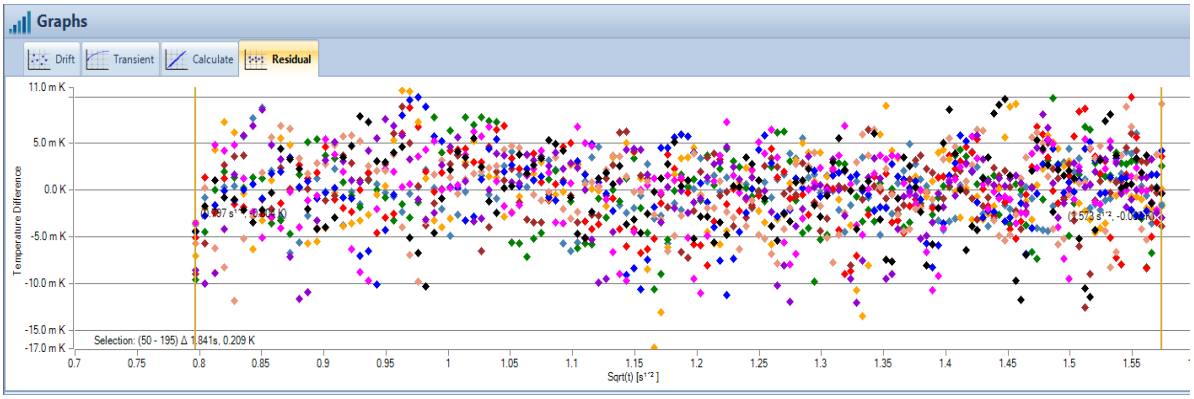

Figure 33. Data points from 50-195.

At the end, after the removal of 50 data points from the front of the analysis, a randomly scattered residual plot is obtained. The fact that we had to remove so many points from the front of the plot indicates that ideal contact is not being made between the sensor and our samples.

3.5 Testing Specific Density

3.5.1 Archimedes Principle

This principle states that an object submerged in a fluid is uplifted by a force that is same as the displaced liquid weight. In this research, it is used to find the density of the 3D printed steel.

$$\text{Specific Gravity} = \frac{W_1}{W_{1\,air} - W_{1\,water}} \quad (5)$$

$$\text{SG} = \frac{Density\ of\ Solid}{Density\ of\ Water} \quad (6)$$

Took two different steel pieces with different weights.

Figure 34. Samples tested for Specific Gravity.

W_1 = 111.5 gm, W1 is the weight of the larger steel piece

W_2 = 31.75 gm, W2 is the weight of the smaller steel piece

Figure 35. Calibrated weights in the air by using a triple beam, sting.

$W_{1\,air}$ = 112.55 gm

$W_{2\,air}$ = 28.95 gm

Figure 36. Weights submerged into a beaker filled with water.

$W_{1\,water}$ = 98.4 gm

$W_{2\,water}$ = 28.95gm

Using Equation (5),

For large sample, SG = 7.87

For small sample, SG = 7.55

Using Equation (6)

The density of water =1 gm/cm³, so SG is equal to density of the solid.

Density for large sample = 7.87 gm/cm³

Density for small sample = 7.55 gm/cm³

Table 8. Densities of different samples (µm-hrs.-ºC).

Sample	W1(gm)	W1 air(gm)	W1 water(gm)	Density of 420 SS (g/cm3)	Calculated Density (g/cm³)
100-3-1120	45.5	47	41.2	7.86	7.84
100-3-1180	42.9	44.2	38.8	7.86	7.94
100-1.5-1120	38.6	39.8	35	7.86	8.04
100-1.5-1180	47.5	48.6	42.8	7.86	8.19
200-1.5-1180	43	44.3	39	7.86	8.11
200-3-1180	44	45.1	39.8	7.86	8.30
200-3-1120	51.5	52.9	46.3	7.86	7.80

The values of densities are used in analyzing the process parameter Sintering Time.

3.5.2 Microstructure

The microstructures for each sample were attained by using a Nikon UM2 microscope. This result helps us see the arrangement of the steel and bronze composition inside the sample. All the other microstructure figures can be found in Appendix C.

Microstructure for 100µm and 200 µm samples are shown below:

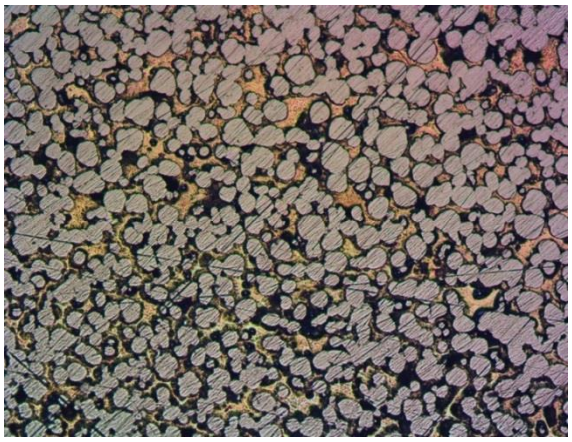

Figure 37. Microstructure for 100µm, 3 hours, 1120 °C.

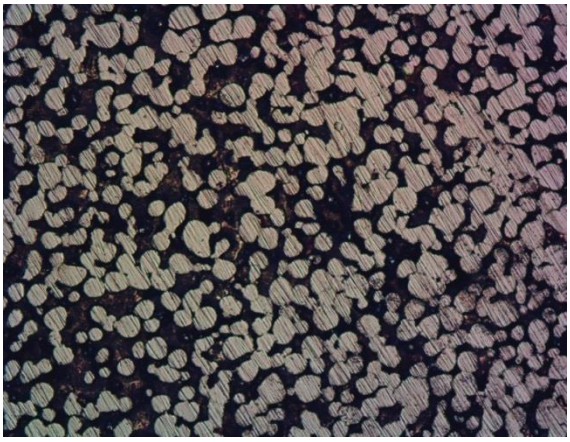

Figure 38. Microstructure for 200µm, 3 hours, 1180 °C.

3.5.3 SEM

SEM stands for Scanning Electron Microscope. The results from SEM help understand more about the microstructure of the specimen as it gives a detailed analysis of specimen topology and composition. In this process, the SEM machine emits electron beam on the top surface of the specimen to give images of material present on the specimen by scanning the area. By scanning the material, the data of each material present in the specimen is calculated and results are given, which have been tabulated below in Table 9. Figure 39 shows the material spread of Fe over the specimen. All the SEM data results can be found in Appendix A,C.

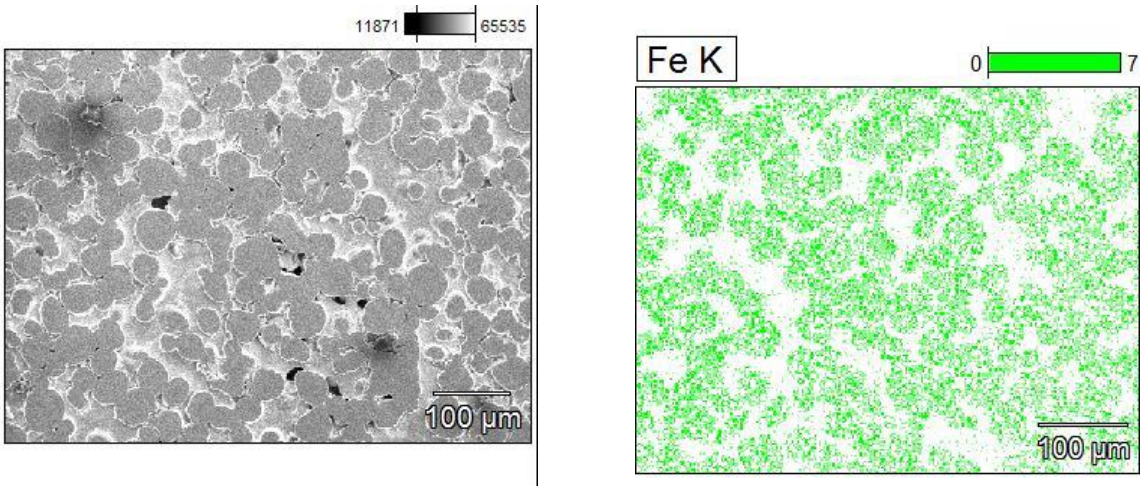

Figure 39. 100µm Sample SEM Result.

Table 9. SEM Results for 100µm, 3 hours, 1120ºC Sample.

Element	Wt. %	Error
C	11.49	0.19
O	0	0
Si	0.60	0.07
Cr	10.12	0.15
Fe	56.02	0.61
Cu	17.77	0.77
Sn	3.80	0.36

Chapter 4: Results and Discussions

This thesis examined the thermal conductivity behavior of stainless steel 420 disks produced by M-Flex 3D Printer. In the additive manufacturing process, it is important to know how thermal properties change with changing process parameters. All the samples showed similar trends in their thermal conductivity change, with changing process parameters. The process parameters taken into consideration are layer thickness, sintering time, and sintering temperature. All the results are analyzed and plotted using Minitab software; the results showed the following paths for thermal conductivity.

Layer thickness: There is a decrease in thermal conductivity value as layer thickness increases, as we can see this in figure 40. Even with a high composition of Bronze in 200µm when compared to 100µm, the value of thermal conductivity decreased because of the microstructure arrangement of Fe and Cu.

Sintering Temperature: There is an increase in the value of thermal conductivity as the sintering temperature increases, which is shown in figure 40. As the sintering temperature increases, there is better diffusion rate between the components, which can be observed in microstructure and SEM results.

Sintering Time: There is a significant effect on thermal conductivity value, as we can see in figure 40; the value of thermal conductivity increased with increase in sintering time, since the effect on thermal conductivity due to sintering time is very high. This is because atom diffusion in solids plays an important role in the sintering process as the time of the sintering

process helps to get higher density; in addition, elevated temperature causes greater diffusion rate. The values of densities can be seen in Table 9.

The graph below shows how layer thickness, sintering temperature and sintering time have an impact on the thermal conductivity value of 3D Printed 420 Stainless Steel.

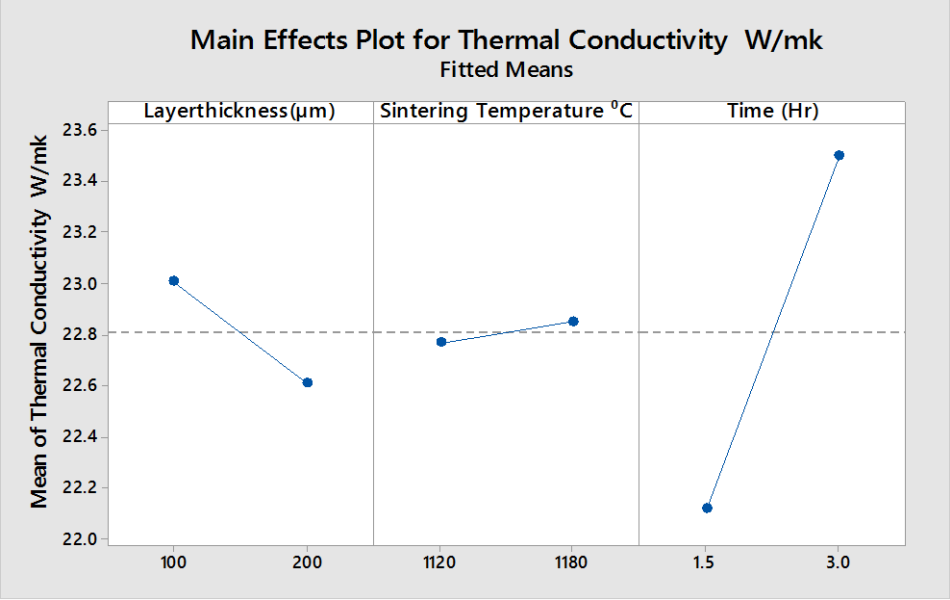

Figure 40. Process parameters Vs. Thermal conductivity.

Interaction plots and plot chart effects are generated to analyze the data obtained for thermal conductivity.

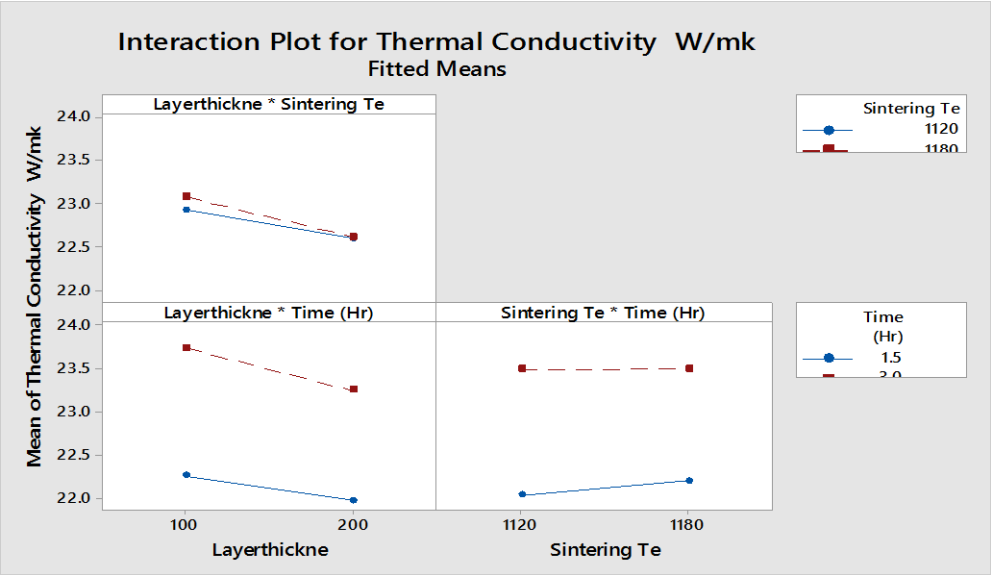

Figure 41. Interaction Plot.

By analyzing all the combinations, a Pareto chart has been generated, which shows the process parameter having the most effect on the thermal conductivity value.

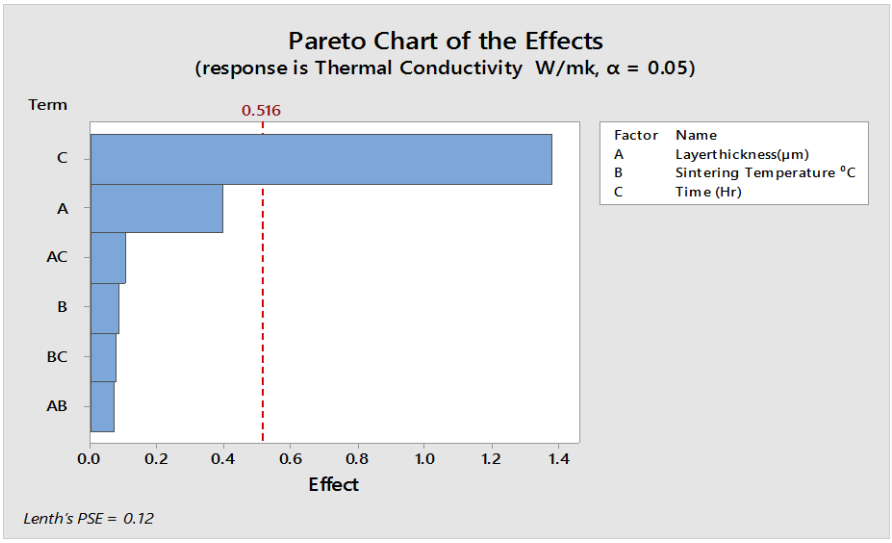

Figure 42. Pareto Chart for Thermal Conductivity Values for different Properties.

The results showed that sintering time has a significant effect on the value of thermal conductivity for AM products.

Chapter 5: Conclusions and Future Works

5.1Conclusions

This thesis examined the thermal conductivity behavior of stainless steel 420 disks produced by M-Flex 3D Printer. In the additive manufacturing process, it is important to know how thermal properties change with changing process parameters. All the samples showed similar trends in thermal conductivity change with changing process parameters. The process parameters taken into consideration are layer thickness, sintering time and sintering temperature. All the results are analyzed and plotted using Minitab software; the results showed the following paths for thermal conductivity:

- The increase in thermal conductivity value is observed significantly in process parameters.
- The highest increase in thermal conductivity value is for 100µm-1180ºC-3hrs specimen, which is seven percent.
- The lowest thermal conductivity is calculated for 200µm-1180ºC-1.5hrs specimen, which is negative three percent.
- There is a decrease in the value of thermal conductivity as the layer thickness increases.
- The value of thermal conductivity increased as the value of sintering time and sintering temperature increased.
- Sintering time has the highest impact on the thermal conductivity value.

5.2 Future Works

The present study helps us realize thermal conductivity behavior of the 420 Stainless Steel made using 3D printing. Additional research needs to be done to find how the microstructure affects the 3D printed parts. During printing process using M-Flex 3D printer, there are many parameters which can affect the thermal conductivity value, such as direction of print and the amount of binder used. Changing parameters can influence the microstructural arrangement.

References:

[1] Totmeier, T.C. and W.F. Gale (Eds). 2004. *Smithells Metals Reference Book*. 3rd ed. ASM: Elsevier.

[2] 2009. *Matweb.* http://matweb.com.

[3] J.P. Holman. 1997. *Heat Transfer*. McGraw-Hill Companies.

[4] Peet, M.J., H.S. Hasan and H.K.D.H. Bhadeshia. Prediction of thermal conductivity of steel.

[5] R.F. Speyer. 1994. "Chapter 9". In *Thermal Analysis of Materials*. New York: Marcel Dekkar.

[6] Yi He. Rapid thermal conductivity measurement with a hot disk sensor.

[7] S.E. Gustafsson and Z. Naturf. 22a (1967), 1005-1011.

[8] Ingenthron, H. Ludwig, T. Joel, K. Agarwal and W. Sealy. Wear Studies in Binder Jet Additive Manufactured Stainless Steel – Bronze Composite C.

[9] Kair, Alexandros Beiker and Konstantions Sofos. Additive Manufacturing and Production of Mettalic Parts in Automotive Industry.

[10] The Effects of Layer Thickness on Dry-Sliding Wear of Binder Jet Additively Manufactured Stainless Steel and Bronze Composite Cody Ingentron.

[11] Gibson, I., D. W. Rosen and B. Stucker. Additive Manufacturing Technologies, Rapid Prototyping to Direct Digital Manufacturing.

[12] http://www.exone.com/Resources/Technology-Overview/What-is-Binder-Jetting

[13] Kulkarni, P.M, Karunakaran K.P, Asim Tewari, Fisseha Legesse, Dhirendra Rana and Alain Bernard. Additive Manufacturing of Directionally Heat Conductive Objects.

[14] Thomas, L.C. *Heat Transfer Professional Version*. 2nd ed. Capstone Publishing Corporation.

[15] Bernal, Julian. Optimization for a heat exchanger application.

[16] Yi He. A transient Plane Source Technique for Rapid Thermal Conductivity Measurement.

[17] http://www.hotdiskinstrumen.com

[18] Roy, R.K. 2001. Design of experiments using the Taguchi Approach. Wiley-Interscience Publication, John Wiley & Sons, Inc.

[19] Kim, Dong-Woo, Myeong-Woo Choo, Tae-II Seo and Eung-Sug Lee. Application of Design of Experiment Method for Thrust Force Minimization in Step-feed Micro Drilling.

Appendix A: Tables of thermal conductivity results and SEM results

Spreadsheet Data 100µm Sample

Table 10. TPS data for 100µm 3 hours 1120ºC sample.

Temperature (ºC)	Thermal Conductivity (W/mK)	Thermal Diffusivity (mm²/s)	Specific Heat (MJ/m³K)
22	23.95	7.24	3.31
22	23.66	6.71	3.53
22	23.43	6.50	3.60
22	23.89	6.37	3.75
22	23.71	7.51	3.16
22	23.89	7.5	3.18
22	23.78	6.86	3.47
22	23.65	6.91	3.42
22	23.45	7.41	3.16
22	23.44	7.28	3.15
22	23.46	7.51	3.16

Table 11. TPS data for 100µm 3 hours 1180ºC sample.

Temperature (ºC)	Thermal Conductivity (W/mK)	Thermal Diffusivity (mm²/s)	Specific Heat (MJ/m³K)
22	23.96	6.64	3.76
22	23.70	7.69	3.29
22	23.64	6.86	3.51
22	23.90	7.69	3.10
22	23.71	5.13	4.53
22	23.89	7.23	3.31
22	23.88	6.40	3.65
22	23.77	6.91	2.87
22	23.68	8.46	3.38
22	23.70	6.81	3.19
22	23.76	6.49	3.51

Table 12. TPS data for 100µm 1.5 hours 1120ºC sample.

Temperature (ºC)	Thermal Conductivity (W/mK)	Thermal Diffusivity (mm^2/s)	Specific Heat (MJ/m^3K)
22	22.28	3.67	6.08
22	22.83	4.93	4.63
22	22.19	4.25	5.23
22	22.68	4.59	4.94
22	22.52	4.58	4.92
22	22.56	4.90	4.61
22	21.17	3.56	5.95
22	21.66	4.49	4.82
22	21.34	3.18	6.71
22	22.59	5.15	4.39
22	21.84	4.20	5.20

Table 13. TPS data for 100µm 1.5 hours 1180ºC sample.

Temperature (ºC)	Thermal Conductivity (W/mK)	Thermal Diffusivity (mm^2/s)	Specific Heat (MJ/m^3K)
22	23.89	8.31	2.88
22	23.90	4.94	4.84
22	23.19	4.23	5.49
22	24.33	5.13	4.78
22	25.79	7.56	3.41
22	24.09	5.40	4.46
22	24.35	4.86	5.01
22	23.40	6.29	3.72
22	23.77	6.57	3.62
22	25.23	6.95	3.63
22	24.18	4.63	5.3

200 µm Sample

Table 14. TPS data for 200µm 3hours 1180ºC sample.

Temperature (ºC)	Thermal Conductivity (W/mK)	Thermal Diffusivity (mm²/s)	Specific Heat (MJ/m³K)
22	22.06	4.19	5.26
22	23.51	7.20	3.26
22	24.90	7.51	3.13
22	24.23	5.54	4.37
22	23.41	4.94	4.74
22	24.75	15.15	1.63
22	24.35	4.93	4.94
22	23.70	6.07	3.90
22	22.21	4.28	5.18
22	22.00	3.75	5.86
22	20.27	2.84	7.13

Table 15. TPS data for 200µm 3 hours 1120ºC sample.

Temperature (ºC)	Thermal Conductivity (W/mK)	Thermal Diffusivity (mm²/s)	Specific Heat (MJ/m³K)
22	23.62	21.20	1.11
22	23.30	20.68	1.13
22	23.34	18.94	1.23
22	23.33	20.33	1.15
22	23.29	19.79	1.18
22	23.30	20.69	1.13
22	23.19	21.01	1.10
22	23.12	20.71	1.12
22	23.15	20.40	1.14
22	23.19	20.26	1.12
22	23.23	20.70	2.84

Table 16. TPS data for 200µm 1.5 hours 1180ºC sample.

Temperature (ºC)	Thermal Conductivity (W/mK)	Thermal Diffusivity (mm^2/s)	Specific Heat (MJ/m^3K)
22	22.13	26.37	0.84
22	22.11	25.20	0.88
22	22.20	24.84	0.89
22	22.21	24.22	0.92
22	21.78	26.98	0.80
22	22.28	22.51	0.99
22	21.85	26.28	0.83
22	21.98	26.49	0.83
22	21.85	26.08	0.84
22	21.80	26.80	0.81
22	22.07	24.90	0.89

SEM Wt. % Results for 100µm and 200µm

Results for 100µm

Table 17. SEM Results for 100µm 3 hours 1120ºC sample.

Element	Wt. %	Error
C	11.49	0.19
Si	0.60	0.07
Cr	10.12	0.15
Fe	56.02	0.61
Cu	17.77	0.77
Sn	3.80	0.36

Table 18. SEM Results for 100µm 3 hours 1180ºC sample.

Element	Wt. %	Error
C	7.76	0.51
Si	0.69	0.09
Cr	12.87	0.22
Fe	62.78	0.84
Cu	8.55	0.88
Sn	7.35	0.56

Table 19. SEM Results for 100µm 1.5 hours 1120ºC sample.

Element	Wt. %	Error
C	3.42	0.40
Si	0.50	0.08
Cr	10.61	0.27
Fe	59.08	0.70
Cu	23.75	0.91
Sn	2.63	0.42

Table 20. SEM Results for 100µm 1.5 hours 1180ºC sample.

Element	Wt. %	Error
C	13311	0.43
Si	0.56	0.04
Cr	10.16	0.25
Fe	55.68	0.63
Cu	16.62	0.78
Sn	3.52	0.39

Results for 200µm

Table 21. SEM Results for 200µm 3 hours 1120ºC sample.

Element	Wt. %	Error
C	5.63	0.39
Si	1.04	0.08
Cr	12.02	0.25
Fe	70.55	0.68
Cu	9.02	0.69
Sn	1.53	0.14

Table 22. SEM Results for 200µm 3 hours 1180ºC sample.

Element	Wt. %	Error
C	1.66	1.36
Si	0	0.00
Cr	10.53	0.93
Fe	55.57	2.25
Cu	22.03	3.25
Sn	10.21	0.74

Table 23. SEM Results for 200µm 1.5 hours 1180ºC sample.

Element	Wt. %	Error
C	11.89	0.64
Si	0.53	0.06
Cr	7.98	0.34
Fe	46.84	0.85
Cu	30.10	01.30
Sn	2.67	0.23

Appendix B: Figures of thermal conductivity results over reference value

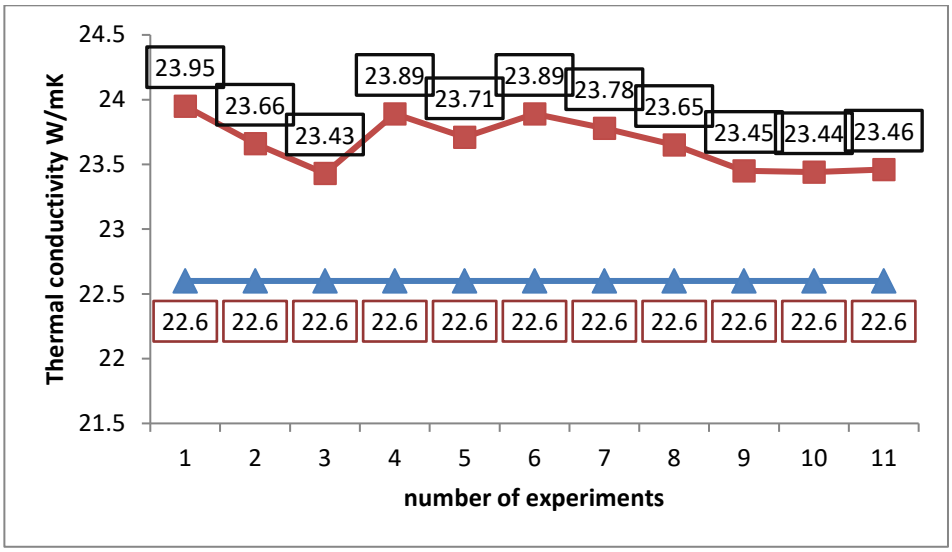

Figure 43. TPS data for 100µm 3 hours 1120ºC sample.

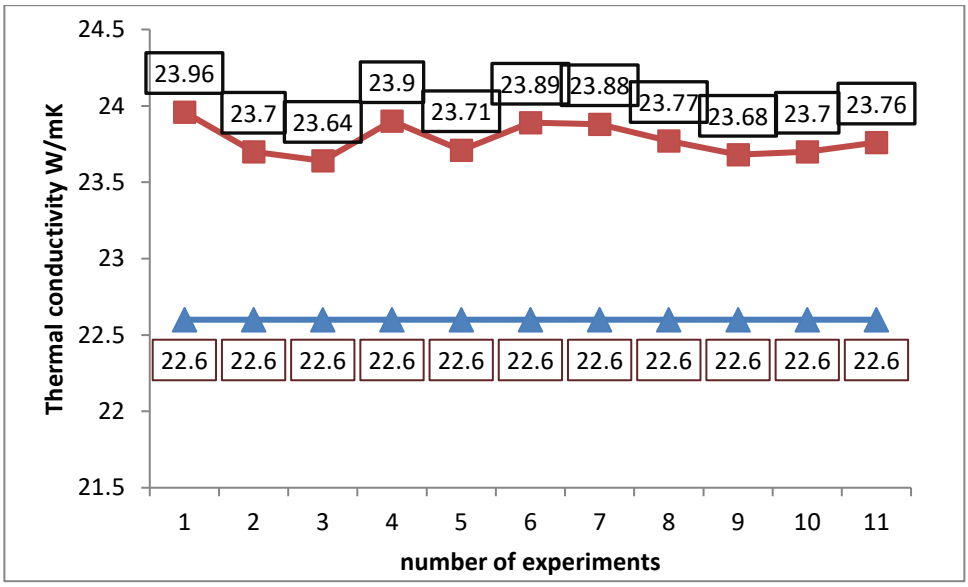

Figure 44. TPS data for 100µm 3 hours 1180ºC sample.

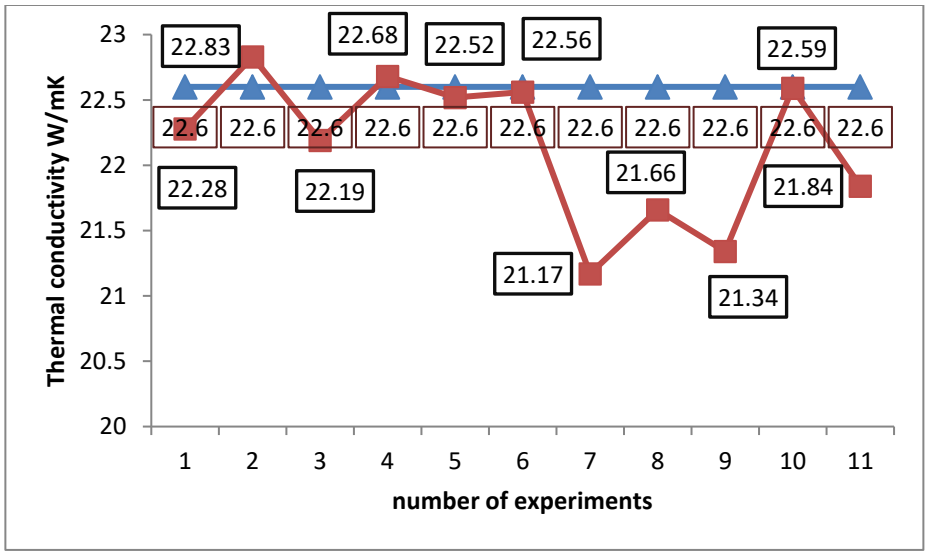

Figure 45. TPS data for 100µm 1.5 hours 1120ºC sample.

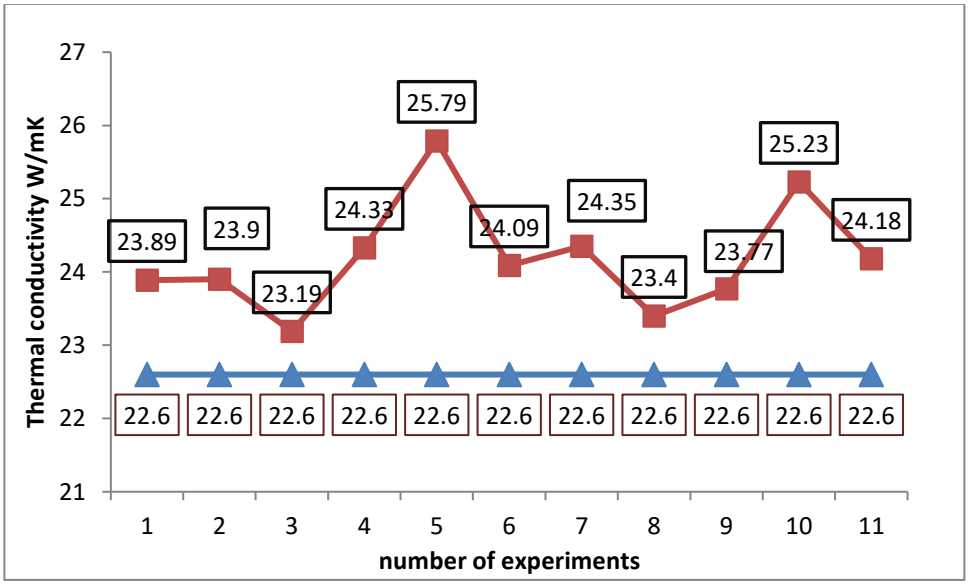

Figure 46. TPS data for 100µm 1.5 hours 1180ºC sample.

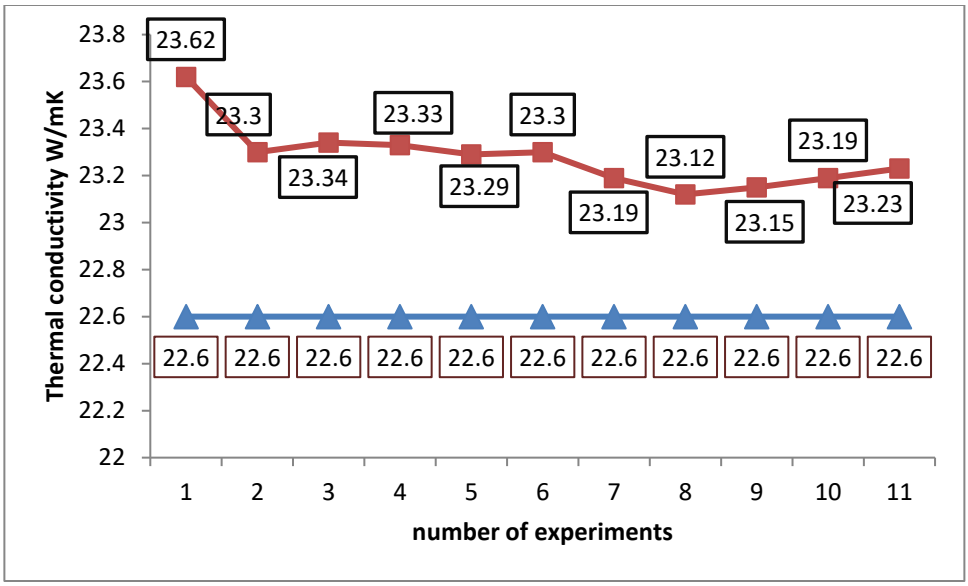

Figure 47. TPS data for 200µm 3 hours 1120ºC sample.

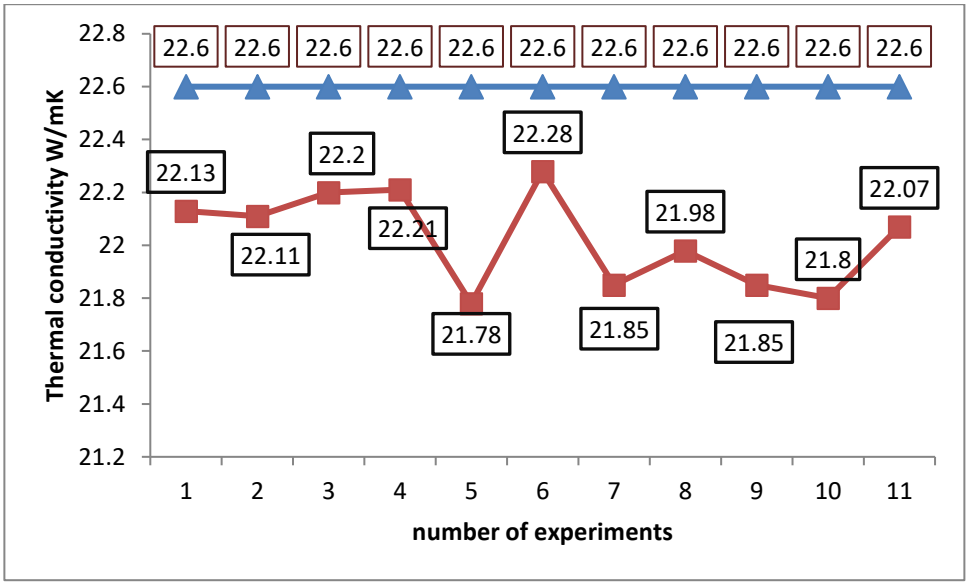

Figure 48. TPS data for 200µm 1.5 hours 1180ºC sample.

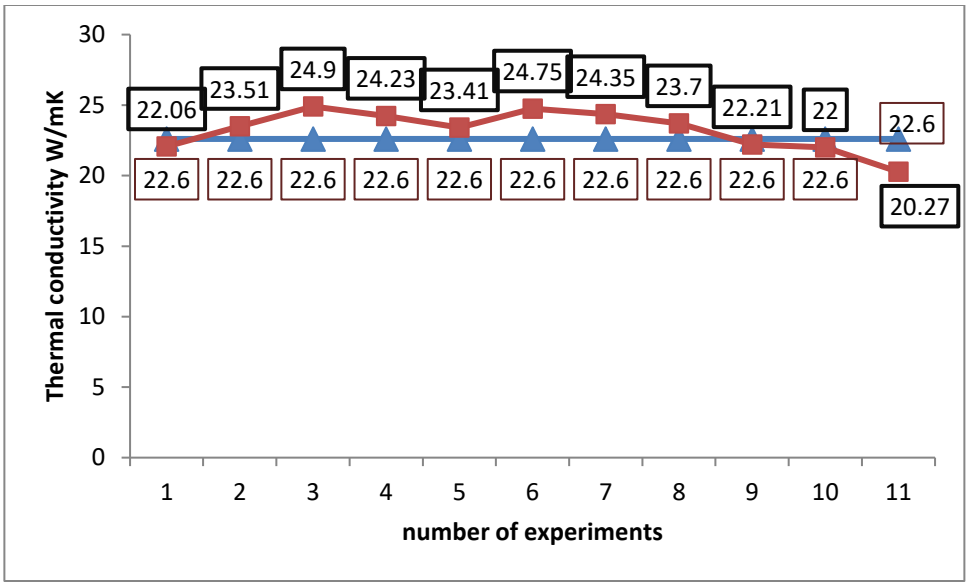

Figure 49. 200µm 3 hours 1180ºC sample.

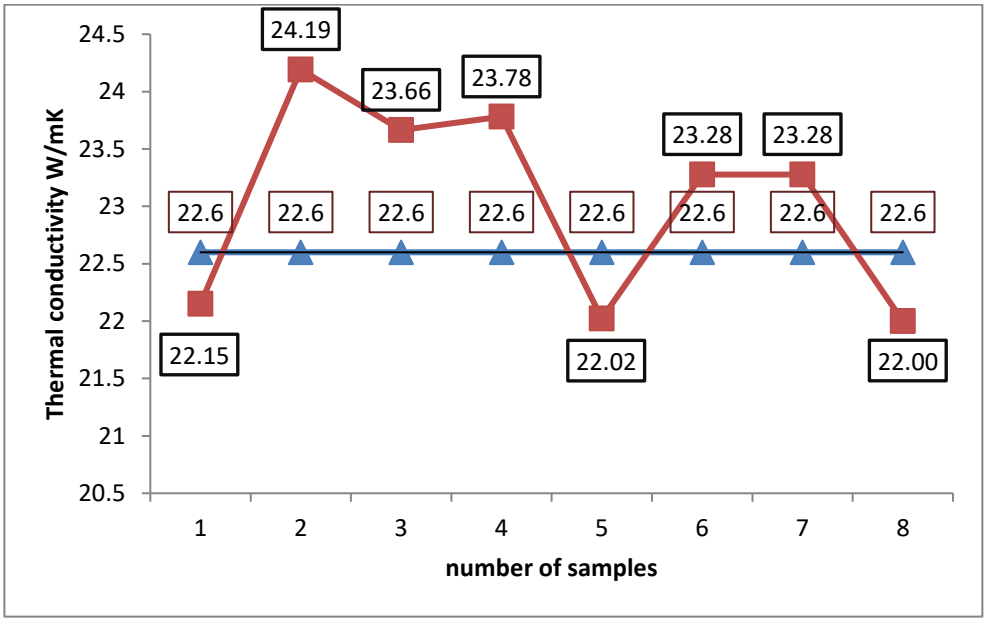

Figure 50. Thermal Conductivity of all Samples vs. Ex One Reference Value.

Appendix C: Microstructure and SEM Figures

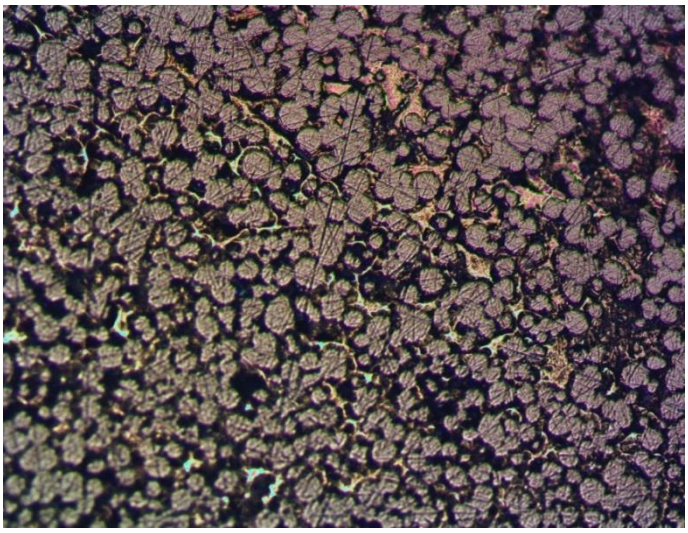

Figure 51. Microstructure for 100µm 1.5 hours 1120 °C.

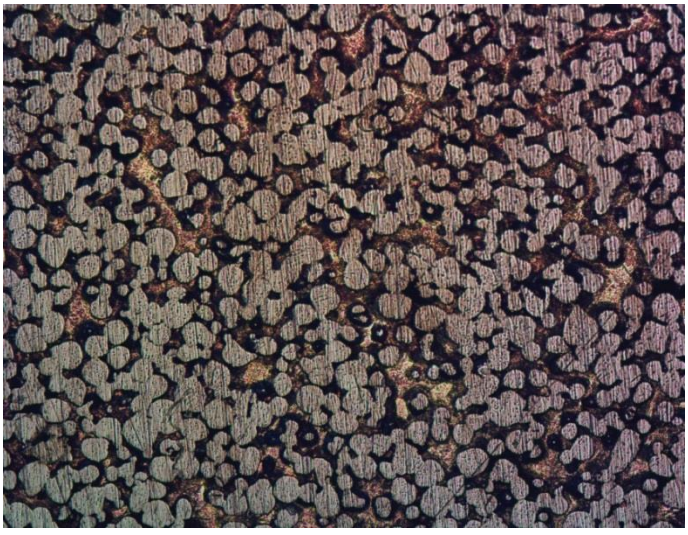

Figure 52. Microstructure for 100µm 1.5 hours 1180 °C.

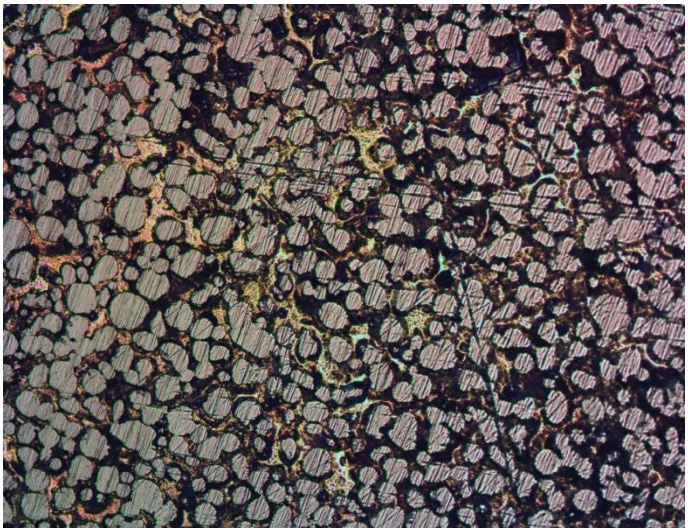

Figure 53. Micro Structure for 200µm 1.5 hours 1180 °C.

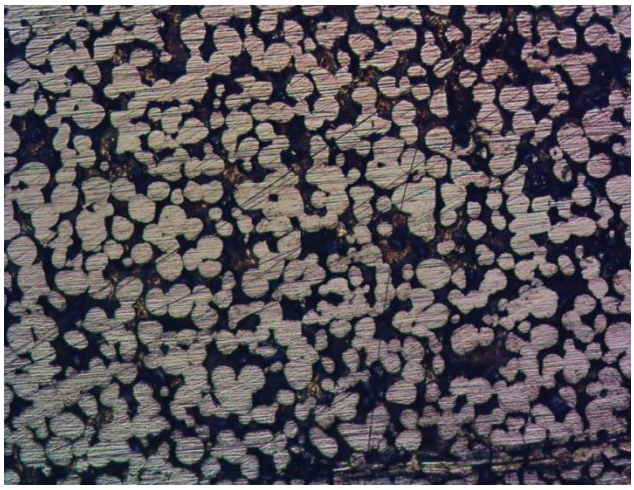

Figure 54. Microstructure for 100µm 3 hours 1180 °C.

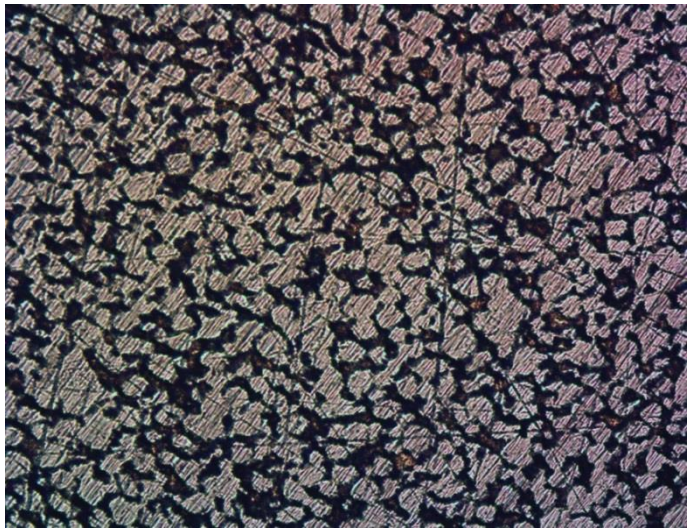

Figure 55. Microstructure for 200µm 3 hours 1120 °C.

SEM data for 100µm 1.5 hours 1120ºC Sample

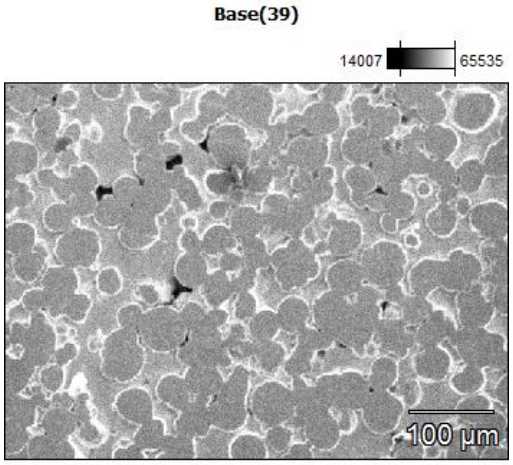

Figure 56. SEM data for 100µm 1.5 hours 1120ºC Sample.

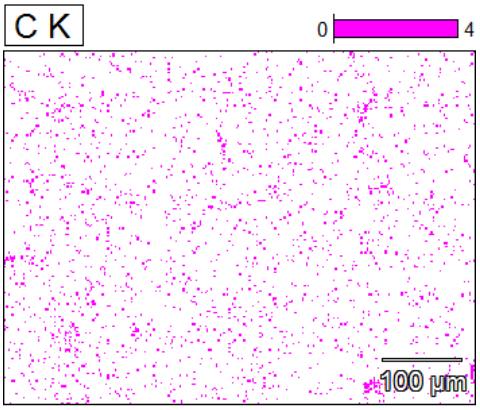

Figure 57. Carbon components on specimen.

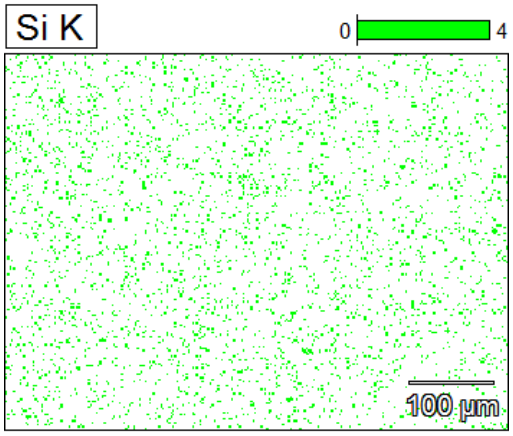

Figure 58. Si content on the specimen.

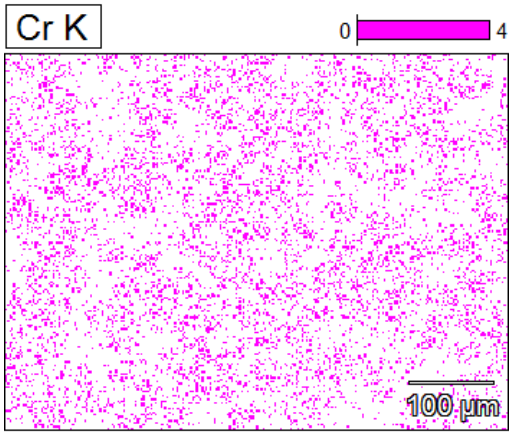

Figure 59. Chromium content over specimen.

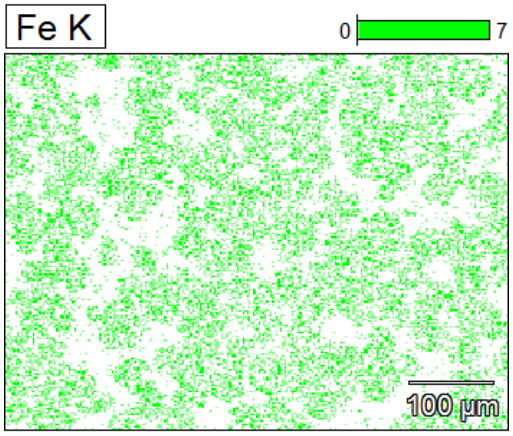

Figure 60. Fe contents over the specimen.

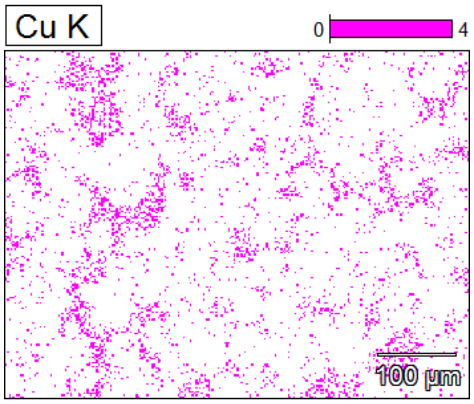

Figure 61. Cu contents over the specimen.

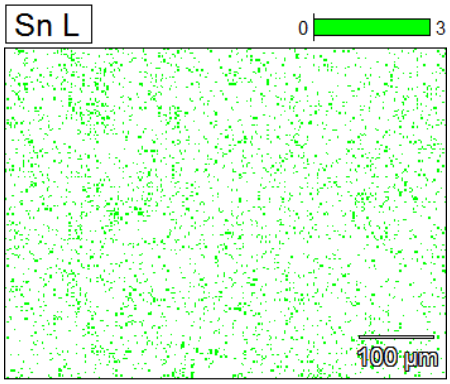

Figure 62. Sn contents over the sample.

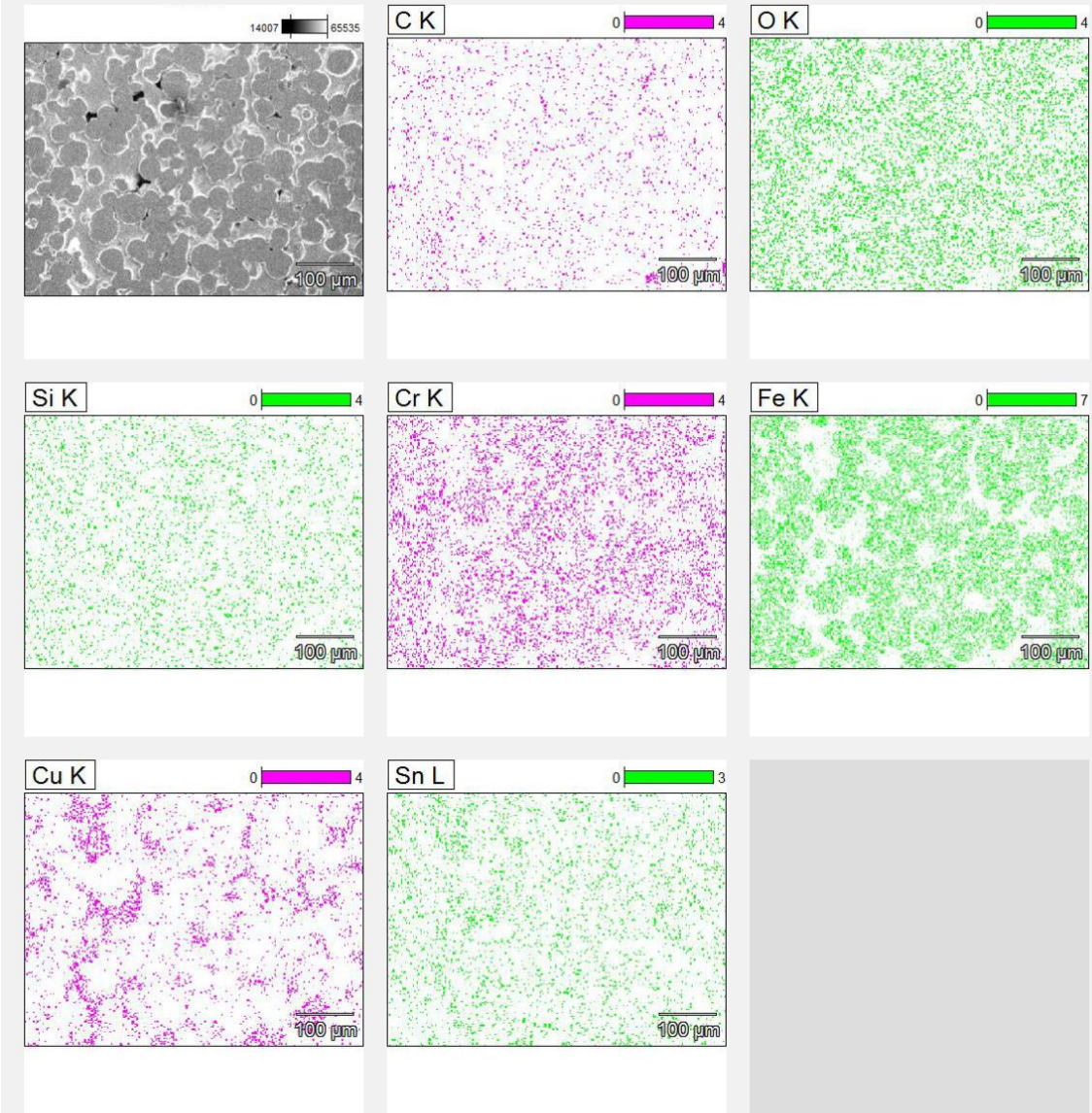

Figure 63. SEM data for 100µm 1.5 hours 1120ºC sample.

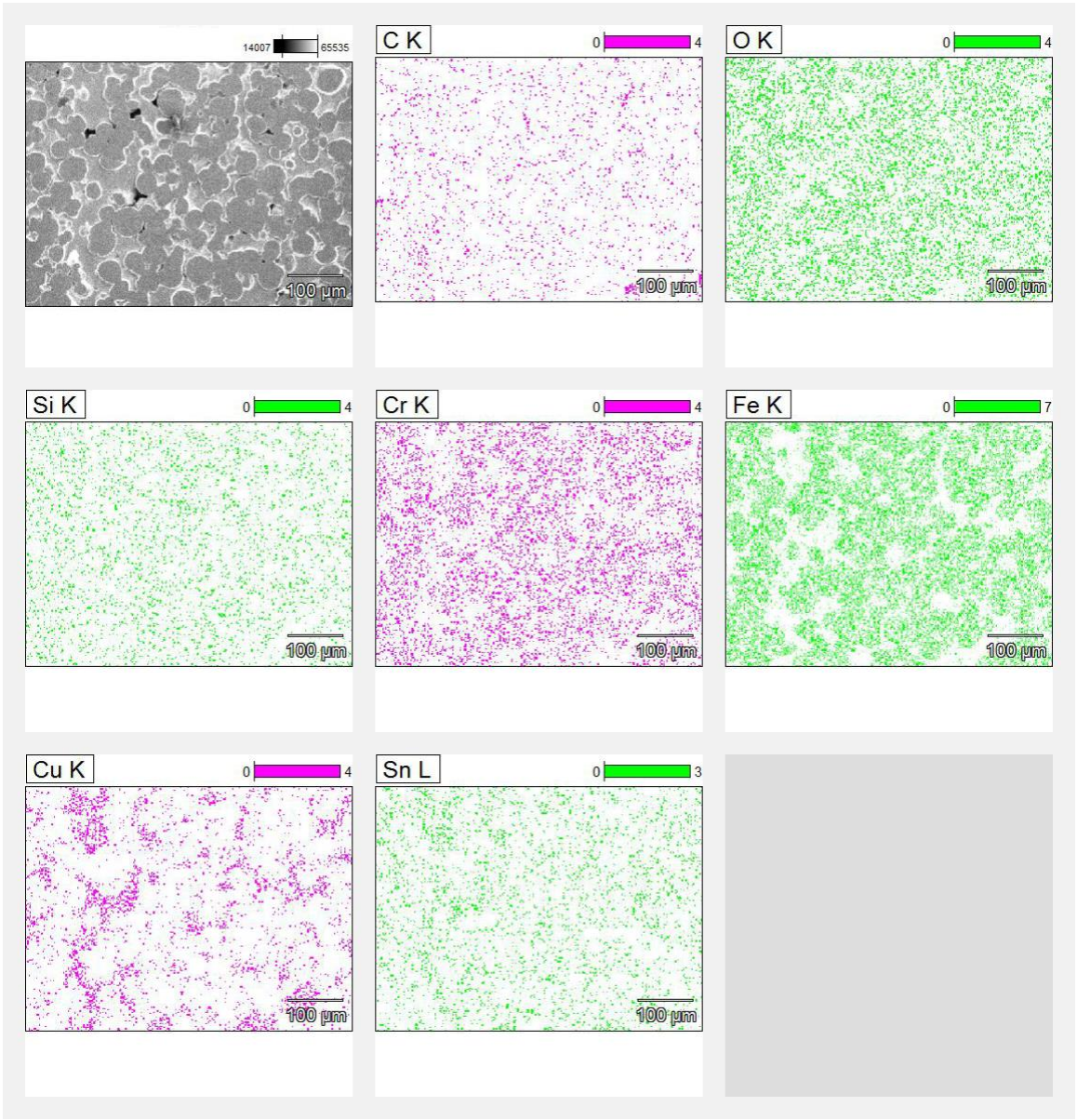

Figure 64. SEM data for 100µm 1.5 hours 1180ºC Sample.

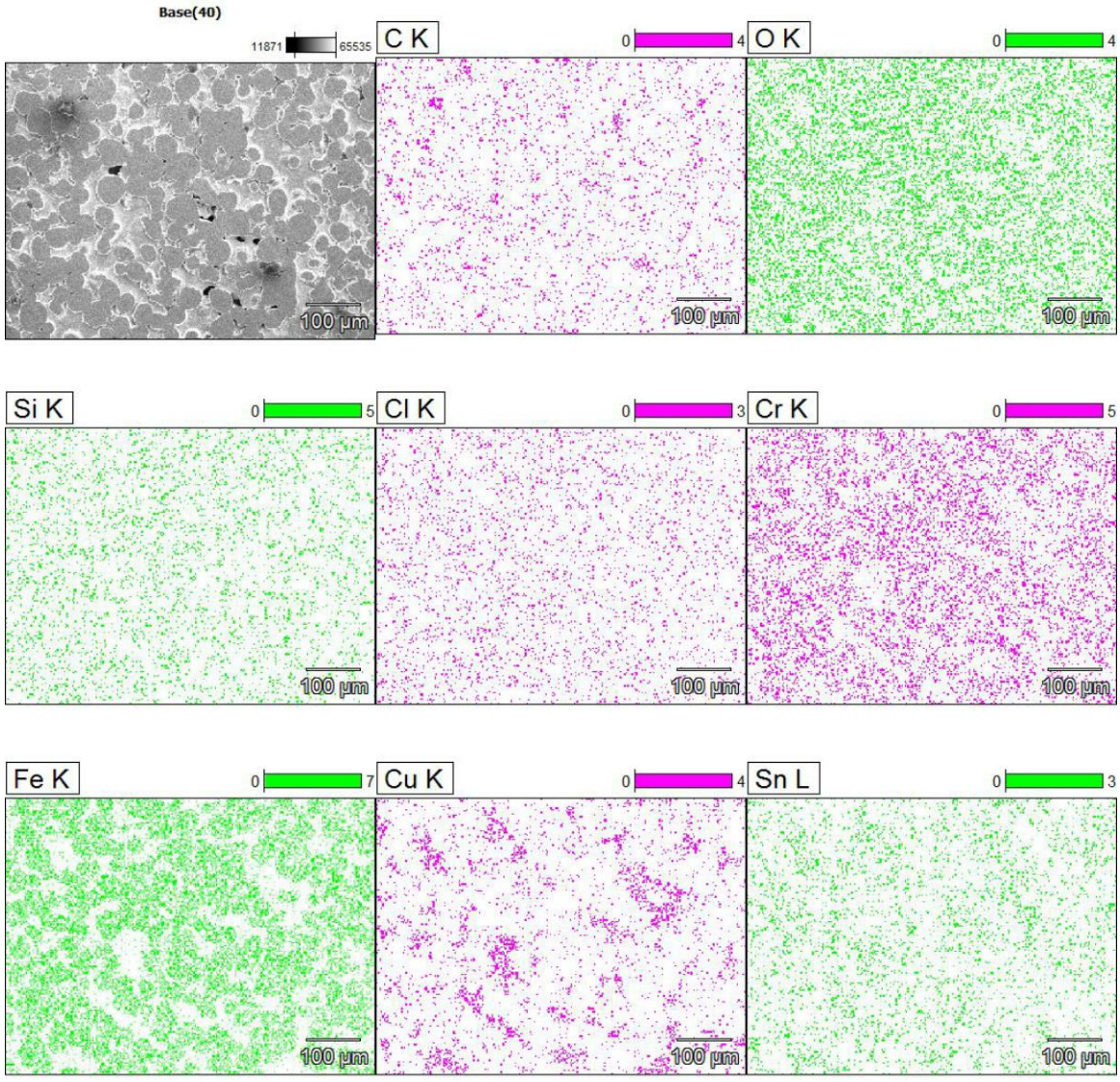

Figure 65. SEM data for 100µm 3 hours 1120ºC sample.

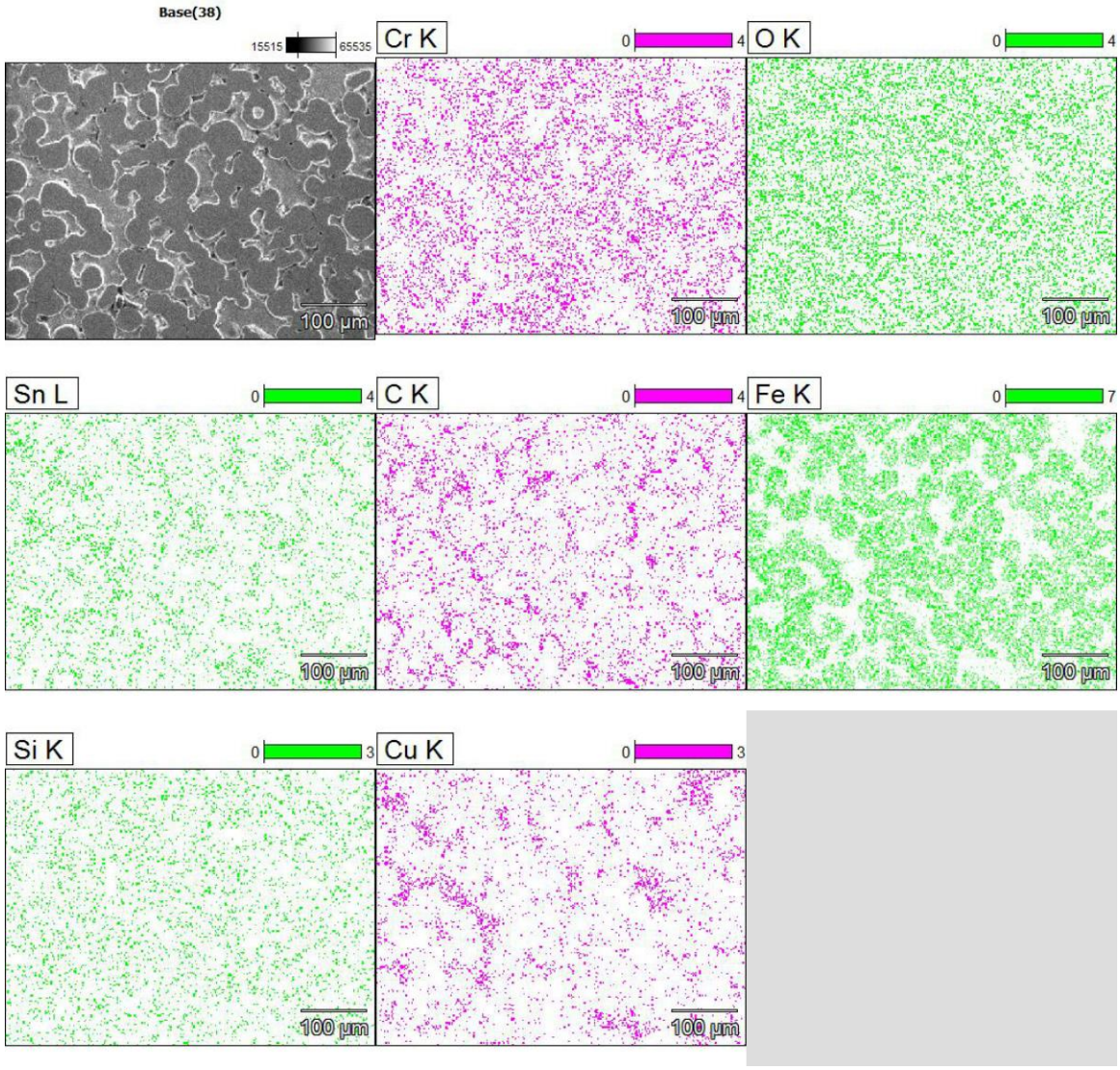

Figure 66. SEM data for 100µm 3 hours 1180ºC sample.

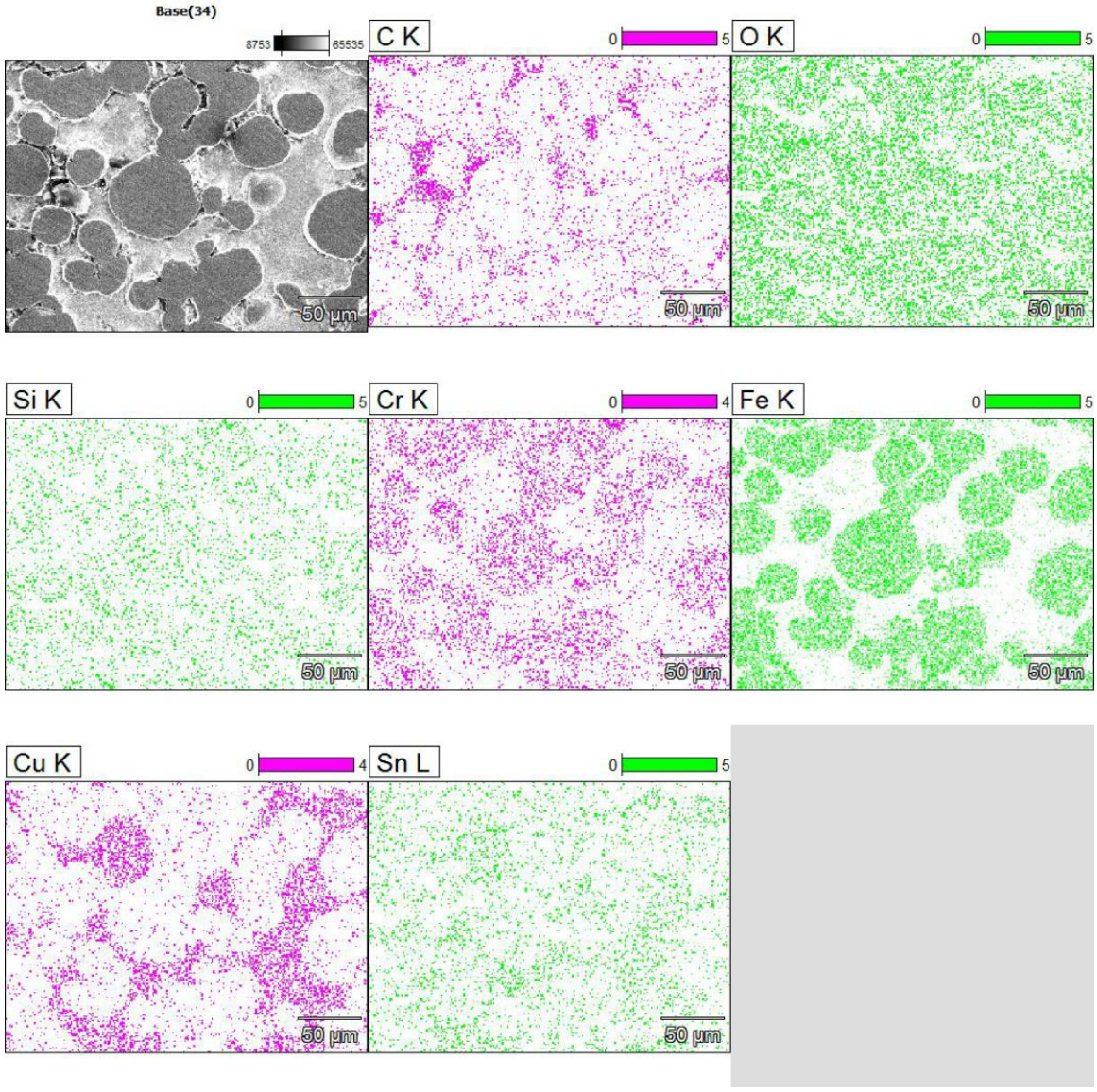

Figure 67. SEM data for 200µm 1.5 hours 1180ºC sample.

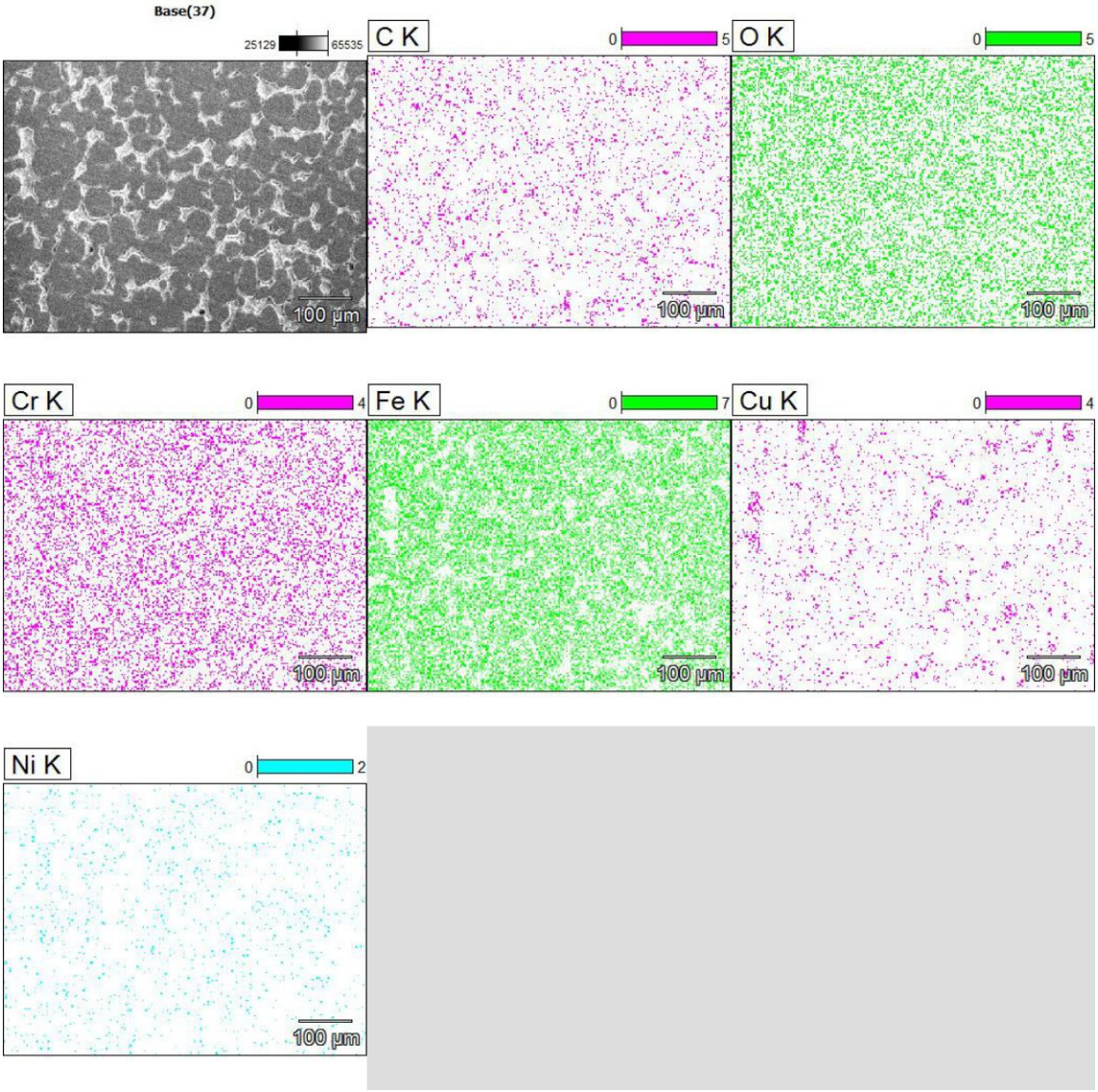

Figure 68. SEM data for 200µm 3 hours 1120ºC sample.

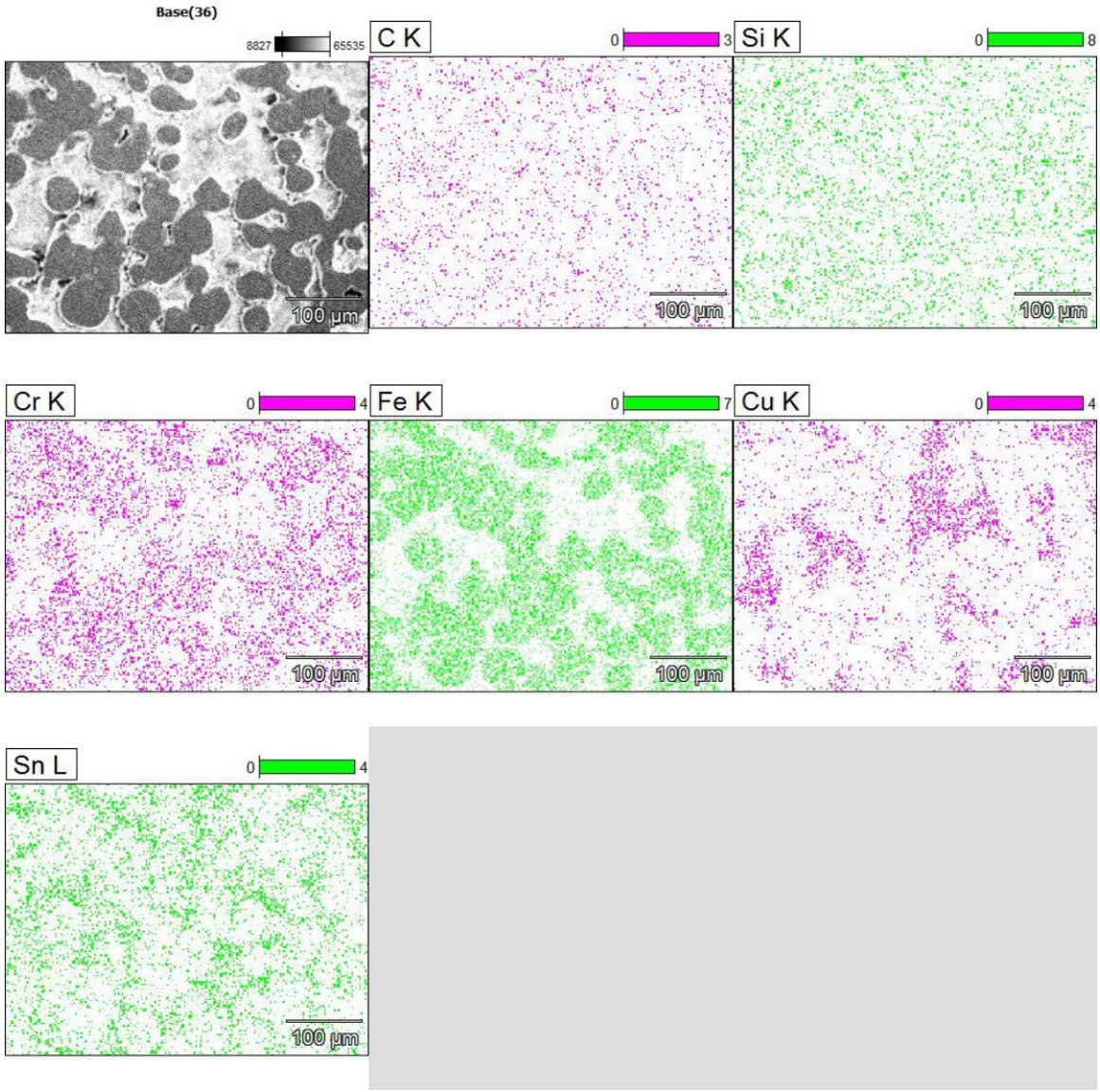

Figure 69. SEM data for 200µm 3hours 1180ºC sample.